PHYSIOME
Published 27 August 2020

The Boron & De Weer Model of Intracellular pH Regulation

Rossana Occhipinti[1*], Soroush Safaei[2], Peter J. Hunter[2], and Walter F. Boron[1,3]

[1]Department of Physiology and Biophysics, Case Western Reserve University, School of Medicine, Cleveland, OH 44106, USA
[2]Auckland Bioengineering Institute, University of Auckland, Auckland, New Zealand
[3]Departments of Medicine and Biochemistry, Case Western Reserve University, School of Medicine, Cleveland, OH 44106, USA

REVIEW

Abstract

The classic Boron and De Weer (1976) paper provided the first evidence of active regulation of pH in cells by an energy-dependent acid-base transporter. These authors also developed a quantitative model — comprising passive fluxes of acid-base equivalents across the cell membrane, intracellular reactions, and an active transport mechanism in the cell membrane (modelled as a proton pump) — to help interpret their measurements of intracellular pH under perturbations of both extracellular CO_2/HCO_3^- and extracellular NH_3/NH_4^+. This *Physiome* paper seeks to make that model, and the experimental conditions under which it was developed, available in a reproducible and well-documented form, along with a software implementation that makes the model easy to use and understand. We have also taken the opportunity to update some of the units used in the original paper, and to provide a few parameter values that were missing in the original paper. Finally, we provide an historical background to the Boron and De Weer (1976) proposal for active pH regulation and a commentary on subsequent work that has enriched our understanding of this most basic aspect of cellular physiology.

Keywords: CO_2, NH_3, squid giant axon, weak acid, weak base

Curated Model Implementation
http://doi.org/10.36903/physiome.12859469

Primary Publications

W. F. Boron and P. De Weer. Intracellular pH transients in squid giant axons caused by CO, NH, and metabolic inhibitors. *Journal of General Physiology*, 67(1):91–112, 1976. ISSN 0022-1295.

OPEN ACCESS
Reproducible Model

Edited by
Karin Lundengård

Curated by
Anand K. Rampadarath

Corresponding author
rxo22@case.edu

Submitted *25 August 2020*

Accepted *25 August 2020*

Citation
Occhipinti et al. (2020) The Boron De Weer Model of Intracellular pH Regulation. Physiome. doi: 10.36903/physiome.12859469

1 Introduction

In 1976 Boron & De Weer published their landmark paper on "Intracellular pH transients in squid giant axons caused by CO_2, NH_3, and metabolic inhibitors" (Boron and De Weer, 1976). The authors used a squid giant axon preparation and a mathematical model of pH buffering and the transport of protons, bicarbonate (HCO_3^-) and CO_2 to establish the experimental evidence for active regulation of intracellular pH (pH_i) by a transporter in the plasma membrane that — at the expense of energy — either moves acid out of the cell, or base into the cell. Today, we refer to such a transporter generically as an acid-extrusion mechanism. For simplicity, Boron & De Weer modelled it as a proton pump, although the result would have been almost indistinguishable had they modelled it as the uptake of HCO_3^- or carbonate (CO_3^{2-}). The paper reported on the consequences of adding and then removing extracellular CO_2/HCO_3^-, NH_3/NH_4^+ (where NH_4^+ is ammonium), or the metabolic inhibitors, cyanide, azide and dinitrophenol (DNP).

In the first experiment, following exposure of the cell to elevated CO_2 and HCO_3^-, CO_2 rapidly enters the cell and intracellular CO_2 equilibrates with the extracellular CO_2, and generates intracellular H^+ and HCO_3^- via the CO_2 hydration reaction ($CO_2 + H_2O \longrightarrow H^+ + HCO_3^-$). The accumulating H^+ results in a rapid fall of pH_i (see Figure 1A & Figure 1B). To the extent that the membrane is permeable to HCO_3^- as well as to CO_2, HCO_3^- will initially enter the cell passively, along its electrochemical gradient. Soon, however, the accumulation of intracellular HCO_3^- reverses the HCO_3^- electrochemical gradient and would be expected to lead to the passive efflux of HCO_3^-. This loss of cellular HCO_3^- would tend to acidify the cell because — to replenish the lost HCO_3^- — additional CO_2 would enter the cell and form even more H^+ and HCO_3^- (the passive CO_2/HCO_3^- shuttle). Thus, the expectation was that prolonged exposure to CO_2 would cause pH_i to fall rapidly (passive influx of CO_2) and then to drift more slowly in the acidic direction (passive efflux of HCO_3^-). In fact, Boron & De Weer observed an *alkaline* drift, leading to the postulate of active extrusion of H^+ — or an equivalent process[1] — at a rate that exceeds the passive shuttling by the CO_2/HCO_3^- couple (see Figure 1A & Figure 1C).

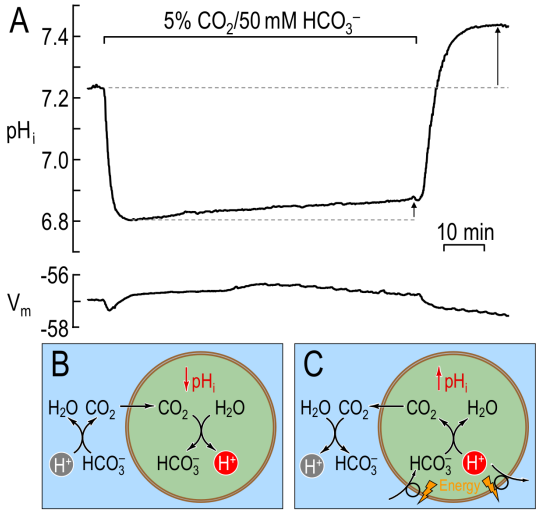

Figure 1. pH_i changes caused by prolonged exposure of a squid giant axon to extracellular CO_2/HCO_3^- in the bulk solution. (**A**) Original pH_i and V_m traces from figure 1 of BDW. Exposing an axon to extracellular CO_2/HCO_3^- causes a rapid fall in pH_i followed by a slow and sustained plateau-phase pH_i recovery (*i.e.*, pH_i rises). Removing extracellular CO_2/HCO_3^- causes pH_i to overshoot its initial resting value. Both the plateau-phase recovery (short arrow) and the overshoot (long arrow) are indicative of net acid extrusion during the period of CO_2/HCO_3^- exposure. (**B**) Cartoon illustrating the processes underlying the initial, rapid acidification phase in (A). The entry of CO_2 leads to the intracellular production of H^+ (and thus to the observed pH_i decay) via the reaction $CO_2 + H_2O \longrightarrow H^+ + HCO_3^-$. (**C**) Cartoon illustrating the processes underlying the plateau-phase alkalinisation in (A). After CO_2 equilibration across the plasma membrane (pH_i nadir in panel (A)), the slow entry of HCO_3^- (or, equivalently, the slow exit of H^+) — which has always been present but was overwhelmed by the influx of CO_2 — leads to the consumption of H^+ (and thus to the observed slow pH_i rise) via the reaction $H^+ + HCO_3^- \longrightarrow CO_2 + H_2O$. The newly formed CO_2 then exits the cell. The observed pH_i overshoot is the result of the accumulation of HCO_3^- during exposure to extracellular CO_2/HCO_3^-. BDW used the mathematical model to postulate the presence of an active acid-extrusion mechanism that would explain both the observed plateau-phase pH_i recovery and the pH_i overshoot. (A), modified from Boron and De Weer (1976). (B)-(C), modified from Boron (2010).

Following removal of external CO_2, intracellular CO_2 diffuses out, while intracellular HCO_3^- combines with H^+ to leave the cell as CO_2. Thus, the entire intracellular H^+ load associated with

[1] Of course, other energy-requiring processes — as yet undiscovered at the time — could also have accounted for the pH_i increase.

CO_2 entry would be removed, returning pH_i to its value before the addition of CO_2/HCO_3^- (or to a slightly lower value, to the extent that HCO_3^- had passively exited during the CO_2/HCO_3^- exposure). In fact, Boron & De Weer observed that pH_i overshoots its resting value by an amount consistent with the net removal of H^+ by the active, acid-extrusion mechanism during the CO_2/HCO_3^- exposure (see Figure 1A & Figure 1C).

In the second experiment, following exposure of the cell to extracellular NH_3/NH_4^+ in the form of NH_4Cl (ammonium chloride), the intracellular environment rapidly becomes alkaline as NH_3 enters and combines with H^+ to form NH_4^+ (equivalent to the hydration of NH_3 to form NH_4^+ and OH^-). If this were the entire story, then pH_i would rise monotonically to a relatively alkaline value, and then the subsequent removal of NH_4Cl would cause pH_i to fall to precisely its initial value. In fact, Boron & De Weer observed that the exposure to NH_4Cl causes pH_i to rise rapidly and then fall slowly. Moreover, the subsequent removal of NH_3/NH_4^+ causes pH_i to undershoot its original value (see Figure 2A). Thus, Boron & De Weer postulated that, during the NH_3/NH_4^+ exposure, NH_4^+ passively enters the cell down its electrochemical gradient. Early during the exposure, this NH_4^+ influx would oppose the NH_3 entry and slightly reduce the pH_i increase. Later during the NH_4Cl exposure, after intracellular $[NH_3]$ rises to match extracellular $[NH_3]$ ($[NH_3]_o$), the continued passive influx of NH_4^+ would generate intracellular H^+ and NH_3. The result would be a slow fall of pH_i and a rise in intracellular $[NH_3]$, the latter leading to the passive exit of NH_3 (the passive NH_3/NH_4^+ shuttle, see Figure 2A & Figure 2B). The experimental data are consistent with the proposed mathematical model.

Finally, exposure of the cells — in turn — to cyanide, DNP and azide resulted in intracellular acidosis, consistent with the accumulation of acid metabolites.

In the present paper, we re-formulate the models from Boron and De Weer (1976), henceforth referred to as 'BDW', and specify the simulation using the Physiome modelling standards CellML (Cuellar et al., 2003) and SED-ML (Bergmann et al., 2017) in order to ensure that the model reproduces the graphs in the original paper and that the model is fully curated.[2] Note that this effort requires the specification of some parameters used in BDW's simulations, but not described in the BDW paper. The curated and annotated model is made available in a form that users can run with OpenCOR[3] to understand the model and to explore the effect of changes in parameter values.

2 pH Buffering by Weak Acids and Weak Bases

We begin by reviewing a few rudimentary concepts of pH buffering by weak acids and bases (Roos and Boron, 1981; Bevensee and Boron, 2013; Boron and Boulpaep, 2016) to provide the background for understanding the derivation and implementation of the BDW model.

Buffers. According to Brönsted's definition (Brönsted, 1923), an acid is any substance that can donate a H^+. Conversely, a base is any substance that can accept a H^+. A buffer is any substance that can reversibly consume or produce H^+, thereby minimising changes in pH.

The dissociation of the uncharged weak acid (HA) to the anionic weak base (A^-) is described by the equilibrium reaction:

$$HA \rightleftharpoons A^- + H^+ \tag{1}$$

which is governed by the equilibrium constant[4]

$$K_{HA} = \frac{[A^-][H^+]}{[HA]}. \tag{2}$$

An example is the carbonic acid (H_2CO_3) dissociation reaction,

$$H_2CO_3 \rightleftharpoons HCO_3^- + H^+.$$

[2] https://models.physiomeproject.org/workspace/5f8

[3] www.opencor.ws

[4] Note that $[A^-]$ denotes a concentration in units of mol $\cdot$ m^{-3} or mM.

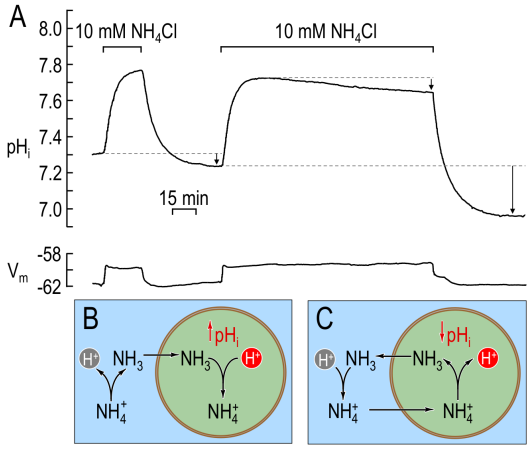

Figure 2. pH_i changes caused by a short and a long exposure of a squid giant axon to extracellular NH_3/NH_4^+ in the bulk solution. (**A**) Original pH_i and V_m traces from figure 2 of BDW. A short exposure of the axon to extracellular NH_3/NH_4^+ causes a rapid rise in pH_i, followed by a pH_i decay that modestly undershoots (lower short arrow) its initial resting value upon removal of extracellular NH_3/NH_4^+. A longer exposure of squid giant axons to extracellular NH_3/NH_4^+ causes a rapid rise in pH_i, followed by a slow and sustained pH_i decay. Removing extracellular NH_3/NH_4^+ causes pH_i to undershoot substantially its initial resting value (long arrow). Both the plateau-phase acidification (upper short arrow) and the undershoot (long arrow) are indicative of net acid loading during the period of NH_3/NH_4^+ exposure. (**B**) Cartoon illustrating the processes underlying the initial alkalinisation phase in (A) for both short and long exposures to extracellular NH_3/NH_4^+. The initial entry of NH_3 leads to the intracellular consumption of H^+ (and thus to the observed pH_i rise) via the reaction $NH_3 + H^+ \longrightarrow NH_4^+$. (**C**) Cartoon illustrating the processes underlying the plateau-phase acidification during the long NH_3/NH_4^+ exposure in (A). After NH_3 equilibration across the plasma membrane (pH_i peak in panel (A)), the slow entry of NH_4^+ — which has always been present but overwhelmed by the influx of NH_3 — leads to the production of H^+ (and thus to the observed slow pH_i decay during the plateau phase) via the reaction $NH_4^+ \longrightarrow NH_3 + H^+$. The newly formed NH_3 then exits the cell. The pH_i undershoots observed upon removal of extracellular NH_3/NH_4^+, during both short and long NH_3/NH_4^+ exposures, are the result of the accumulation of NH_4^+ during exposure to extracellular NH_3/NH_4^+. BDW used the mathematical model to postulate the above sequence of events, including both the plateau-phase acidification and the pH_i undershoot. (A), modified from Boron and De Weer (1976). (B)-(C), modified from Boron (2010).

The total weak acid concentration, [TA], is the sum of [HA] and [A^-]. Note that [TA] is one of the two main unknowns in the BDW model for weak acids.

The dissociation of the cationic weak acid (BH^+) to the uncharged weak base (B) is described by the equilibrium reaction,

$$BH^+ \rightleftharpoons B + H^+, \tag{3}$$

where the equilibrium constant is

$$K_{BH} = \frac{[B][H^+]}{[BH^+]}. \tag{4}$$

An example is the NH_4^+ dissociation reaction,

$$NH_4^+ \rightleftharpoons NH_3 + H^+.$$

The total weak base concentration, [TB], is the sum of [BH^+] and [B]. Note that [TB] is one of the two main unknowns in the BDW model for weak bases.

The CO_2/HCO_3^- buffer pair. The formation of HCO_3^- and H^+ from CO_2 by hydration is given by the equilibrium reaction

$$CO_2 + H_2O \rightleftharpoons HCO_3^- + H^+,$$

where the equilibrium constant is

$$K_{CO_2} = \frac{[HCO_3^-][H^+]}{[CO_2]}. \tag{5}$$

Taking logarithms of both sides of Equation 5, and recognising from Henry's law that

$$[CO_2] = s \cdot p_{CO_2}, \tag{6}$$

where s is the solubility coefficient for CO_2 and p_{CO_2} is the partial pressure of CO_2, we obtain the familiar Henderson-Hasselbalch equation

$$pH = pK_{CO_2} + \log \frac{[HCO_3^-]}{s \cdot p_{CO_2}}. \tag{7}$$

Here, $pH = -\log[H^+]$[5] and $pK_{CO_2} = -\log(K_{CO_2})$.

In terms of the nomenclature above, one might regard CO_2 as the weak acid HA[6], and HCO_3^- as its conjugate base A^-.

Buffering power (β). By definition, β is the amount of strong base (*e.g.*, NaOH), or the negative of the amount of strong acid (*e.g.*, HCl), that one must add to 1 L of solution to raise pH by one pH unit:

$$\beta = \frac{\Delta[\text{Strong Base}]}{\Delta pH} = -\frac{\Delta[\text{Strong Acid}]}{\Delta pH}. \tag{8}$$

The units of β are mM. For additional details, refer to Roos and Boron (1981); Boron and Boulpaep (2016). Note that BDW defined β as a negative number, as did Koppel and Spiro in their original definition of buffering (Koppel, 1914; Roos and Boron, 1980), rather than as a now-conventional positive quantity, as did Van Slyke in his later work (Van Slyke, 1922). BDW's definition, which they consistently applied, has no effect on the outcome of their simulations. In the present paper, we will follow the definition of Van Slyke — defining β as a positive number — and make appropriate sign changes to the derived equations.

3 The Boron & De Weer Model for the Permeation by an Uncharged Weak Acid and its Conjugate, Anionic Weak Base

The BDW mathematical model consists of two time-dependent ordinary differential equations (ODEs), one describing the time-course of the concentration of total intracellular buffer ($[TA]_i = [HA]_i + [A^-]_i$) and the other the time-course of the intracellular free H^+ concentration (which is related to pH_i). BDW derived these two equations for the general cases in which any buffer pair HA/A^-, or any buffer pair B/BH^+, can move passively across the plasma membrane of a prototype cell. Then, they applied these two general equations to their specific experimental conditions, namely exposure of a cell (a squid giant axon) to equilibrated extracellular CO_2/HCO_3^- or to equilibrated extracellular NH_3/NH_4^+.

Here, following BDW's approach, we begin by deriving the equations for HA/A^-. In the next section, we apply the same general formalism to B/BH^+.

[5] The definition of pH as a pH scale based on powers of 10 was introduced by Sørensen in an attempt to simplify the notation of $[H^+]$ and to avoid having to resort to decimals for tiny amounts of $[H^+]$ (Sørensen, 1909).

[6] Note that although CO_2 is often regarded as an acid, the true weak acid is H_2CO_3, the product of the reaction of CO_2 with H_2O.

Derivation for weak acids. Imagine that a cell is exposed to a solution containing equilibrated HA/A^- and that both HA and A^- initially move into the cell — because of the chemical gradient in the case of HA, and because of the electrochemical gradient in the case of A^-.

An integrated form of Fick's first law of diffusion describes the net passive influx[7] of HA (J_{HA})

$$J_{HA} = P_{HA}\Big([HA]_o - [HA]_i\Big), \tag{9}$$

where J_{HA} is flux ($mol \cdot m^{-2} \cdot s^{-1}$) and P_{HA} ($m \cdot s^{-1}$) is the membrane permeability to the uncharged weak acid HA. Note that this is a passive diffusion equation because HA is uncharged.

The constant field equation — also known as the Goldman, Hodgkin, Katz (GHK) (Goldman, 1943; Hodgkin and Huxley, 1952) equation — describes the net passive influx of A^- (J_{A^-}):

$$J_{A^-} = P_{A^-}\left(\frac{V_m F}{RT}\right)\left(\frac{[A^-]_o - \epsilon[A^-]_i}{1-\epsilon}\right), \tag{10}$$

where P_{A^-} ($m \cdot s^{-1}$) is the membrane permeability to the charged conjugate base A^-, V_m is the membrane potential (intracellular relative to extracellular potential), and ϵ is a shorthand for $e^{-V_m F/RT}$. Note that J_{HA} and J_{A^-} have units of $mol \cdot m^{-2} \cdot s^{-1}$.

Although HA and A^- can interconvert in the cytosol, BDW assumed that the intracellular concentration of total weak acid $[TA]_i$ only can change due to the transmembrane fluxes of HA and A^- (see Figure 3). Thus, the time rate of change of $[TA]_i$ is

$$\frac{d[TA]_i}{dt} = \rho\,(J_{HA} + J_{A^-}), \tag{11}$$

where ρ (m^{-1}) is the area-to-volume ratio for the cell, and converts the transmembrane flux per unit area (in units of $mol \cdot m^{-2} \cdot s^{-1}$) to a time rate of change per unit cell volume ($mol \cdot m^{-3} \cdot s^{-1}$ or $mM \cdot s^{-1}$). Equation 11 is the first of two ODEs of the BDW model for the buffer pair HA/A^-.

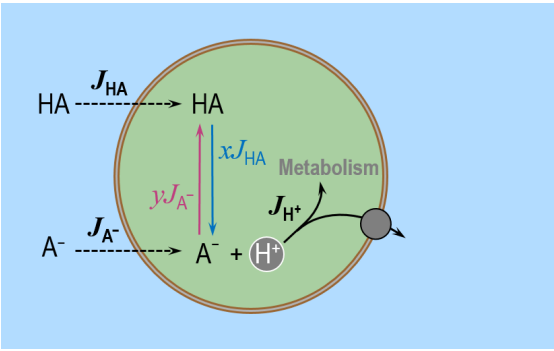

Figure 3. Cartoon illustrating the main assumptions in the BDW model of permeating uncharged weak acid HA and its conjugate anionic weak base A^-. The BDW model consists of two time-dependent ODEs. The first one describes the time-course of the intracellular concentration of total weak acid $[TA]_i$, and the second one describes the time-course of $[H^+]_i$. BDW assumed that $[TA]_i$ changes in time because of the transmembrane fluxes of HA (J_{HA}) — modelled according to Fick's first law of diffusion — and A^- (J_{A^-}) — modelled according to the Goldman, Hodgkin, Katz (GHK) equation. According to BDW, the time rate of change of $[H^+]_i$ depends on the net rate dQ/dt at which acids are added into the cytosol. BDW assumed that dQ/dt depends on (i) the release of H^+ by some fraction x of the entering HA (*i.e.*, xJ_{HA}), (ii) the consumption of H^+ by some fraction y of the entering A^- (*i.e.*, yJ_{A^-}), and (iii) the additional rate of intracellular H^+ consumption via metabolism or active acid extrusion (J_{H^+}).

Later, Bevensee and Boron defined the time rate of change per unit volume (*e.g.*, $d[TA]_i/dt$) as a 'pseudoflux' ϕ, with the area-to-volume ratio folded into the value of ϕ (Bevensee and Boron,

[7] BDW used M to denote a transmembrane flux. In the present paper, we use the more widely used notation J.

2013). Physiologists sometimes prefer to present experimental data in terms of pseudoflux because most mammalian cells often have complex geometries that make it difficult to estimate surface area.

In deriving the second ODE of their model, BDW started by noting that the time rate of change of free protons, $\mathrm{d}[\mathrm{H}^+]_\mathrm{i}/\mathrm{d}t$, depends on the rate at which acids are added into the cytosol per unit volume and per unit time — denoted $\mathrm{d}Q/\mathrm{d}t$ ($\mathrm{mol}\cdot\mathrm{m}^{-3}\cdot\mathrm{s}^{-1}$) where Q is the total intracellular acid content. Like $\mathrm{d}[\mathrm{TA}]_\mathrm{i}/\mathrm{d}t$, both $\mathrm{d}[\mathrm{H}^+]_\mathrm{i}/\mathrm{d}t$ and $\mathrm{d}Q/\mathrm{d}t$ are pseudofluxes.

In their simple system of a squid giant axon exposed to CO_2 (*i.e.*, HA) and HCO_3^- (*i.e.*, A^-), BDW assumed that only three general processes affect $\mathrm{d}Q/\mathrm{d}t$: (i) the release of H^+ by some fraction (x) of the entering HA (*i.e.*, xJ_HA), (ii) the consumption of H^+ by some fraction (y) of the entering A^- (*i.e.*, yJ_{A^-}), and (iii) the "additional" rate of intracellular consumption or active extrusion of H^+ (J_{H^+}; see Figure 3) above the fixed background rate of H^+ extrusion necessary to balance the fixed background rate of acid loading (*i.e.*, addition of H^+ or equivalent acid, or removal of OH^- or equivalent base) in the absence of HA/A^-. Thus,

$$\frac{\mathrm{d}Q}{\mathrm{d}t} = \rho\left(xJ_\mathrm{HA} - yJ_{\mathrm{A}^-} - J_{\mathrm{H}^+}\right). \tag{12}$$

A critical insight by BDW is that during each infinitesimal increment in time during which a bolus of HA enters the cell, the entering HA redistributes itself between HA (and H^+) vs A^-, according to the pre-existing ratios $[\mathrm{HA}]_\mathrm{i}/[\mathrm{TA}]_\mathrm{i}$ and $[\mathrm{A}^-]_\mathrm{i}/[\mathrm{TA}]_\mathrm{i}$. Thus, the fraction y of entering HA that remains HA is

$$y = \frac{[\mathrm{HA}]_\mathrm{i}}{[\mathrm{TA}]_\mathrm{i}} = \frac{[\mathrm{HA}]_\mathrm{i}}{[\mathrm{HA}]_\mathrm{i} + [\mathrm{A}^-]_\mathrm{i}}. \tag{13}$$

This is also the fraction of entering A^- that combines with H^+ and becomes HA. Combining the above expression with Equation 2,

$$y = \frac{[\mathrm{HA}]_\mathrm{i}}{[\mathrm{HA}]_\mathrm{i} + [\mathrm{A}^-]_\mathrm{i}} = \frac{[\mathrm{H}^+]_\mathrm{i}}{[\mathrm{H}^+]_\mathrm{i} + K_\mathrm{HA}} = \alpha, \tag{14}$$

which BDW defined as α. Conversely, the fraction x of A^- that remains A^- is

$$x = \frac{[\mathrm{A}^-]_\mathrm{i}}{[\mathrm{HA}]_\mathrm{i} + [\mathrm{A}^-]_\mathrm{i}}. \tag{15}$$

This is also the fraction of entering HA that dissociates to form A^- and H^+. Combining the above expression with Equation 2,

$$x = \frac{[\mathrm{A}^-]_\mathrm{i}}{[\mathrm{HA}]_\mathrm{i} + [\mathrm{A}^-]_\mathrm{i}} = \frac{K_\mathrm{HA}}{[\mathrm{H}^+]_\mathrm{i} + K_\mathrm{HA}} = 1 - \alpha. \tag{16}$$

In summary, Equation 12 becomes:

$$\frac{\mathrm{d}Q}{\mathrm{d}t} = \rho\Big((1-\alpha)J_\mathrm{HA} - \alpha J_{\mathrm{A}^-} - J_{\mathrm{H}^+}\Big). \tag{17}$$

BDW modelled J_{H^+} ($\mathrm{mol}\cdot\mathrm{m}^{-2}\cdot\mathrm{s}^{-1}$) as the additional proton-extrusion rate above the fixed background rate

$$J_{\mathrm{H}^+} = \begin{cases} \dfrac{k}{\rho}\Big([\mathrm{H}^+]_\mathrm{i} - [\mathrm{H}^+]_\mathrm{i}'\Big) & \mathrm{pH}_\mathrm{i} < \mathrm{pH}_\mathrm{i}', \\ 0 & \text{otherwise}, \end{cases} \tag{18}$$

where k (s^{-1}) is the proton-pumping rate constant, $(k/\rho)[\mathrm{H}^+]_\mathrm{i}$ is the additional flux of H^+ above the background H^+ flux of $(k/\rho)[\mathrm{H}^+]_\mathrm{i}'$, which occurs at the resting $[\mathrm{H}^+]_\mathrm{i}$ of $[\mathrm{H}^+]_\mathrm{i}'$ (*i.e.*, resting pH_i

of pH_i'). Note that k/ρ has units of $(m \cdot s^{-1})$, consistent with the membrane permeability terms P_{HA} and P_{A^-} in Equation 9 and Equation 10.[8]

The BDW authors used the definition of buffering power, in its infinitesimal form, to derive the relation between $d[H^+]_i/dt$ and dQ/dt, as shown in the following steps.

Our first goal is to obtain an expression for dpH/dt in terms of dQ/dt. According to the chain rule:

$$\frac{dpH}{dt} = \left(\frac{dpH}{dQ}\right)\left(\frac{dQ}{dt}\right). \tag{19}$$

By definition (see Equation 8), $\beta = -dQ/dpH$ $(mol \cdot m^{-3})$, or equivalently

$$\frac{dpH}{dQ} = -\frac{1}{\beta}. \tag{20}$$

Combining Equation 19 and Equation 20

$$\frac{dpH}{dt} = \left(-\frac{1}{\beta}\right)\left(\frac{dQ}{dt}\right). \tag{21}$$

Our next goal is to obtain an expression for $\frac{dpH}{dt}$ in terms of $\frac{d[H^+]_i}{dt}$. According to the chain rule:

$$\frac{dpH}{dt} = \left(\frac{dpH}{d[H^+]_i}\right)\left(\frac{d[H^+]_i}{dt}\right). \tag{22}$$

By definition, $pH = -\ln [H^+]_i/2.303$, so that:

$$\frac{dpH}{d[H^+]_i} = -\frac{1}{2.303[H^+]_i}. \tag{23}$$

Combining Equation 22 and Equation 23, we have

$$\frac{dpH}{dt} = \left(-\frac{1}{2.303[H^+]_i}\right)\left(\frac{d[H^+]_i}{dt}\right), \tag{24}$$

or equivalently,

$$\frac{d[H^+]_i}{dt} = -2.303[H^+]_i\left(\frac{dpH}{dt}\right). \tag{25}$$

Substituting Equation 21 into Equation 25, we obtain

$$\frac{d[H^+]_i}{dt} = \left(\frac{2.303[H^+]_i}{\beta}\right)\left(\frac{dQ}{dt}\right). \tag{26}$$

Finally, substituting Equation 17 into Equation 26,

$$\frac{d[H^+]_i}{dt} = \left(\frac{2.303[H^+]_i}{\beta}\right)\rho\Big((1-\alpha)J_{HA} - \alpha J_{A^-} - J_{H^+}\Big), \tag{27}$$

which is the second equation of the BDW model.

Substituting for α (from Equation 14), $[HA]_i = \alpha[TA]_i$, $[A^-]_i = (1-\alpha)[TA]_i$, in Equation 11 and Equation 27, we obtain the two ODEs of the BDW model in terms of $[TA]_i$ and $[H^+]_i$:

$$\frac{d[TA]_i}{dt} = \rho\,(J_{HA} + J_{A^-}), \tag{28}$$

[8] In the BDW paper, the final equation before the Appendix had a typographical error, omitting the ρ in the following equation: $M_H = (k/\rho)([H^+] - [H^+]')$, where M_H is a flux (today represented as J_H). Indeed, WFB had included ρ in his extant Fortran code.

$$\frac{d[H^+]_i}{dt} = \left(\frac{2.303[H^+]_i}{\beta}\right)\rho\left(\left(\frac{K_{HA}}{[H^+]_i + K_{HA}}\right)J_{HA} - \left(\frac{[H^+]_i}{[H^+]_i + K_{HA}}\right)J_{A^-} - J_{H^+}\right), \tag{29}$$

where J_{HA} (from Equation 9), and J_{A^-} (from Equation 10) are given by:

$$J_{HA} = P_{HA}\left([HA]_o - \frac{[H^+]_i}{[H^+]_i + K_{HA}}[TA]_i\right),$$

$$J_{A^-} = P_{A^-}\left(\frac{V_m F}{RT}\right)\left(\frac{[A^-]_o - \frac{K_{HA}}{[H^+]_i + K_{HA}}[TA]_i\epsilon}{1-\epsilon}\right),$$

and J_{H^+} is given by Equation 18.

The numerical solution of the above two equations yields the time courses of $[TA]_i$ and $[H^+]_i$, which in turn yield the time-courses of $[HA]_i$ and $[A^-]_i$ via:

$$[HA]_i = \alpha[TA]_i, \tag{30}$$

$$[A^-]_i = (1-\alpha)[TA]_i, \tag{31}$$

where

$$\alpha = \frac{[H^+]_i}{[H^+]_i + K_{HA}}. \tag{32}$$

Simulation for CO_2/HCO_3^- experiments. BDW employed Equation 28 and Equation 29 to simulate the experiments in which they exposed a squid giant axon to a solution containing equilibrated CO_2/HCO_3^-. Their simulation protocol was a step change in (a) extracellular p_{CO_2} from 0 to 5% CO_2 (37 mmHg or, with $s = 0.0321$ mM · mmHg^{-1}, $[CO_2]_o = s.p_{CO_2} = 1.1877$ mM) and (b) extracellular $[HCO_3^-]$ from 0 to 59.5260 mM (the value that $[HCO_3^-]_o$ has in a solution containing 5% CO_2 at pH_o of 7.70)[9]. The step change is applied for 2700 s (45 min) at constant $pH_o = 7.70$.

Table 1 and Table 2 report the parameter values used by BDW. Table 1 provides parameter values that are common to both the CO_2/HCO_3^- and the NH_3/NH_4^+ experiments. Table 2 provides parameter values exclusive to the CO_2/HCO_3^- experiments only.

In the present work, the differential Equation 28 and Equation 29 — when coded in CellML and solved with OpenCOR — produce the plots in Figure 4. The simulation file Boron-CO2.sedml contains the computational setting for running the model. Open the .sedml file in OpenCOR and click Run Simulation. The initial conditions are $[TA]_i = 0$ mM and $pH_i = 7.40$. Note that Figure 4 illustrates the time courses not only of pH_i — as presented by BDW — but also of quantities (*e.g.*, various solute concentrations and fluxes) not displayed in the original paper; these values are useful for understanding the processes that contribute to the pH_i transient. Moreover, our curated and annotated version of the BDW model also allows one to alter the parameter values from those originally chosen by BDW, thereby extending the ability of the user to investigate the predictive power of the computational model.

[9] BDW arrived at the value $[HCO_3^-]_o = 59.5260$ mM by rearranging the equilibrium relation for CO_2/HCO_3^- outside the cell: $[HCO_3^-]_o = \frac{K_{CO_2}[CO_2]_o}{[H^+]_o} = 59.5260$ mM, when $K_{CO_2} = 1 \times 10^{-3}$ mM (or equivalently, $pK_{CO_2} = -\log(K_{CO_2}) = 6.0$), $[CO_2]_o = 1.1877$ and $pH_o = 7.70$.

Table 1. Parameter values used in both simulations of squid-axon CO_2/HCO_3^- experiments and NH_3/NH_4^+ experiments.

Symbol	Name	BDW Value	Unit	New Value	Unit
T	temperature	23 (296.15)	°C (°K)		
R	gas constant	8.314	$J \cdot mol^{-1} \cdot K^{-1}$		
F	Faraday constant	96485	$C \cdot mol^{-1}$		
ρ	area/volume ratio	0.008[1]	μm^{-1}	8000	m^{-1}
pH_o	extracellular pH	7.70			

[1] Note that BDW did not report the value of ρ, but rather the value of the fiber (*i.e.*, axon) diameter, which is equal to 500 μm and corresponds to a ρ of 0.008 μm^{-1} or 8000 m^{-1}.

Table 2. Parameter values for simulations of squid-axon CO_2/HCO_3^- experiments.

Symbol	Name	BDW Value	Unit	New Value	Unit
β_{CO_2}	buffering power	−26	mM	26	mM
s	solubility constant for CO_2	0.0321 [1]	mM/mmHg	0.241	mM/KPa
p_{CO_2}	partial pressure of CO_2	37	mmHg	4.933	KPa
p_{CO_2}	partial pressure of CO_2	37	mmHg	4.933	KPa
$[CO_2]_o$	extracellular CO_2	1.1877	mM		
$[HCO_3^-]_o$	extracellular HCO_3^-	59.5260	mM		
P_{CO_2}	membrane permeability	6×10^{-3}	$cm \cdot s^{-1}$	6×10^{-5}	$m \cdot s^{-1}$
$P_{HCO_3^-}$	membrane permeability	5×10^{-7}	$cm \cdot s^{-1}$	5×10^{-9}	$m \cdot s^{-1}$
K_{CO_2}	acid dissociation constant	10^{-3}	mM		
pK_{CO_2}	acid dissociation constant	6.0			
V_m	membrane potential	−57 [2]	mV	−0.057	V
k	H^+ pump rate constant	0 – 300 [3]	s^{-1}		
pH_i	intracellular pH	7.40			
pH_i'	basal pH	7.30 [4]			

[1] Note that BDW did not report the value of s. This value is inferred from a p_{CO_2} of 37 mmHg (reported in the legend of BDW's figure 6) and a $[CO_2]_o$ of 1.1877 mM (in the original Fortran code). Although BDW reported a value for s of 0.0346 mM/mmHg (taken from Harned and Davis (1943), referring to 0.5 M NaCl at 20°C), they used this value only for the Davenport diagram in their figure 5A.

[2] BDW did not report the value of V_m, but in the Fortran code, used −57 mV, which matched the measured mean value.

[3] In figure 6A of the BDW paper, the proton pumping rate constant (k) had values of 0, 10, 75, 150, or 300 s^{-1}.

[4] BDW did not report this value, but in their code used 7.30.

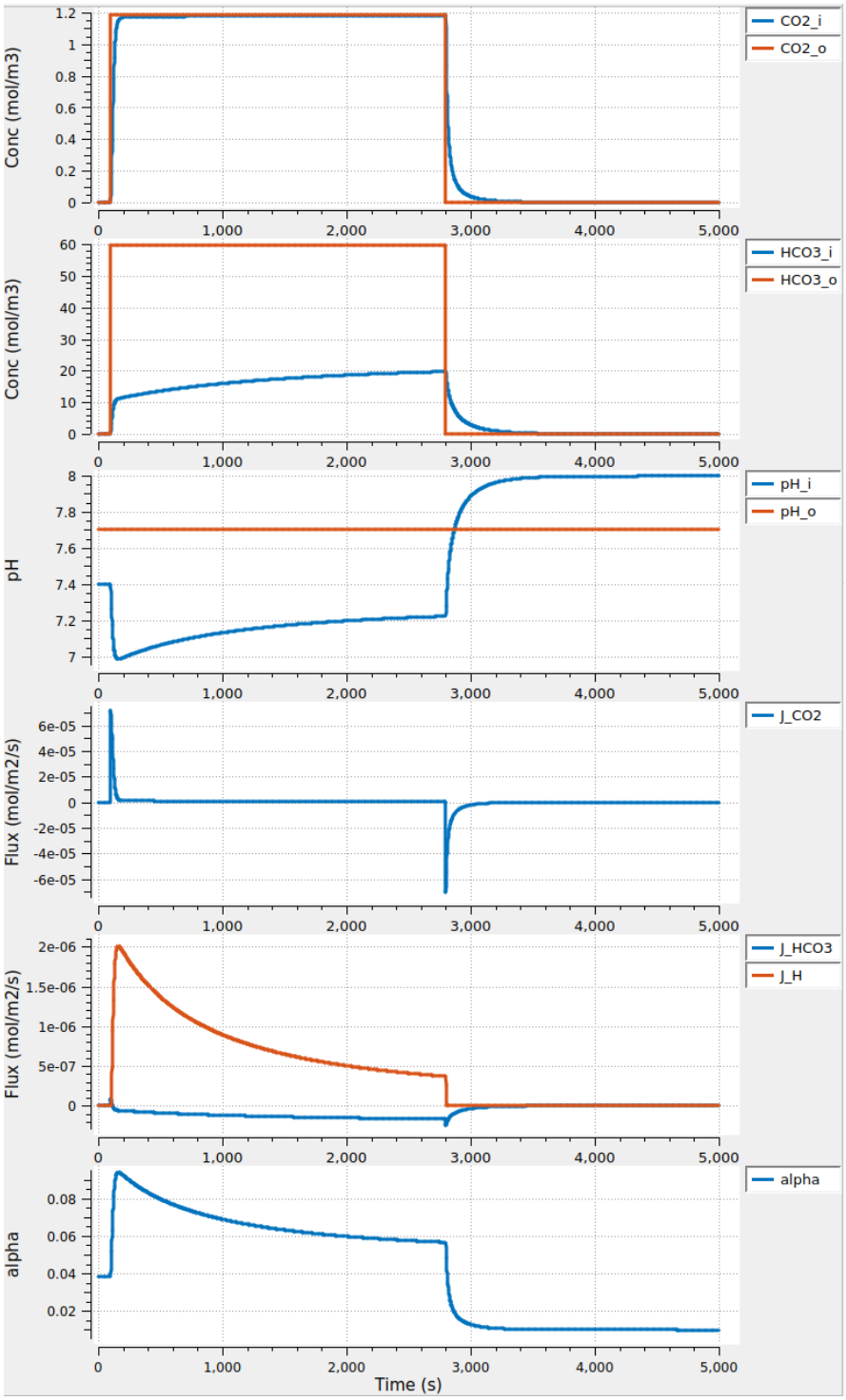

Figure 4. Solution of the BDW model during and following a 2700 s period of externally applied CO_2. In these simulations $pH_o = 7.70$ and $[HCO_3^-]_o$ is determined from the equilibrium with $[H^+]_o$ and CO_2 (footnote 9). Note that, during the plateau phase, $[HCO_3^-]_i$ continues to rise as pH_i rises at a constant $[CO_2]_i$ (the proton pumping rate k is set to 300 s^{-1}, thus $k/\rho = 0.0375\ m \cdot s^{-1}$). Note also that, after the removal of CO_2/HCO_3^-, pH_i rises to a higher value (~ 8.15) than its starting value (~ 7.4), indicating the net extrusion of acid from the cell during the CO_2/HCO_3^- exposure.

4 The Boron & De Weer Model for the Permeation by an Uncharged Weak Base and its Conjugate, Cationic Weak Acid

Following an approach analogous to the one outlined above for weak acids, BDW derived two time-dependent ODEs. The first describes the time-course of the concentration of total intracellular buffer ($[TB]_i = [B]_i + [BH^+]_i$), and the other the time-course of the intracellular free $[H^+]_i$, for any buffer pair B/BH^+.

Derivation for weak bases. Imagine that a cell is exposed to a solution containing equilibrated B/BH^+, and that both B and BH^+ initially move into the cell — because of the chemical gradient in the case of B, and because of the electrochemical gradient in the case of BH^+.

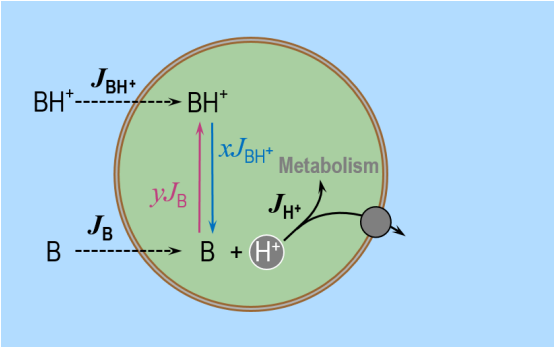

Figure 5. Cartoon illustrating the main assumptions in the BDW model of permeating uncharged weak base B and its conjugate anionic weak acid BH^+. The BDW model consists of two time-dependent ODEs. The first one describes the time-course of the intracellular concentration of total weak base $[TB]_i$, and the second one describes the time-course of $[H^+]_i$. BDW assumed that $[TB]_i$ changes in time because of the transmembrane fluxes of HA (J_B) — modelled according to Fick's first law of diffusion — and BH^+ (J_{BH^+}) — modelled according to the Goldman, Hodgkin, Katz (GHK) equation. According to BDW, the time rate of change of $[H^+]_i$ depends on the net rate dQ/dt at which acids are added into the cytosol. BDW assumed that dQ/dt depends on (i) the release of H^+ by some fraction x of the entering BH^+ (*i.e.*, xJ_{BH^+}), (ii) the consumption of H^+ by some fraction y of the entering B (*i.e.*, yJ_B), and (iii) the additional rate of intracellular H^+ consumption via metabolism or active acid extrusion (J_{H^+}).

Assuming, as in Figure 5, that $[TB]_i$ only can change due to the transmembrane fluxes of B (J_B) and BH^+ (J_{BH^+}), the time rate of change of $[TB]_i$ — analogous to Equation 11 above — is

$$\frac{d[TB]_i}{dt} = \rho\,(J_B + J_{BH^+})\,, \tag{33}$$

where ρ (m^{-1}) is again the area-to-volume ratio for the cell. The equation

$$J_B = P_B\Big([B]_o - [B]_i\Big), \tag{34}$$

is an integrated form of Fick's first law of diffusion that describes the net passive flux of B, and

$$J_{BH^+} = P_{BH^+}\left(\frac{V_m F}{RT}\right)\left(\frac{[BH^+]_o - \epsilon'[BH^+]_i}{\epsilon' - 1}\right), \tag{35}$$

describes the net passive influx of BH^+ according to the GHK equation. In the previous two equations, P_B ($m \cdot s^{-1}$) is the membrane permeability to the uncharged weak base B, P_{BH^+} ($m \cdot s^{-1}$) is the membrane permeability to the charged conjugate weak acid BH^+, and ϵ' is a shorthand for $e^{V_m F/RT}$. Equation 33 is the first of two ODEs of the BDW model for the buffer pair B/BH^+.

The second equation of the BDW model for a weak base — analogous to Equation 27 above — is

$$\frac{d[H^+]_i}{dt} = \left(\frac{2.303[H^+]_i}{\beta}\right)\rho\Big((1-\alpha)J_{BH^+} - \alpha J_B - J_{H^+}\Big), \tag{36}$$

where J_{H+} is the same as in Equation 18 and

$$\alpha = \frac{[BH^+]_i}{[BH^+]_i + [B]_i} = \frac{[H^+]_i}{[H^+]_i + K_{BH^+}}, \tag{37}$$

and

$$1 - \alpha = \frac{[B]_i}{[BH^+]_i + [B]_i} = \frac{K_{BH^+}}{[H^+]_i + K_{BH^+}}. \tag{38}$$

Substituting for α, $[BH^+]_i = \alpha[TB]_i$, $[B]_i = (1-\alpha)[TB]_i$, J_{BH^+} , J_B in Equation 33 and Equation 36, we obtain the two ODEs of the BDW model in terms of $[TB]_i$ and $[H^+]_i$

$$\frac{d[TB]_i}{dt} = \rho\left(J_B + J_{BH^+}\right), \tag{39}$$

$$\frac{d[H^+]_i}{dt} = \frac{2.303[H^+]_i}{\beta}\rho\left(\left(\frac{K_{BH^+}}{[H^+]_i + K_{BH^+}}\right)J_{BH^+} - \left(\frac{[H^+]_i}{[H^+]_i + K_{BH^+}}\right)J_B - J_{H^+}\right), \tag{40}$$

where

$$J_{BH^+} = P_{BH^+}\left(\frac{V_m F}{RT}\right)\left(\frac{[BH^+]_o - \frac{[H^+]_i}{[H^+]_i + K_{BH^+}}[TB]_i\epsilon'}{\epsilon' - 1}\right),$$

$$J_B = P_B\left([B]_o - \frac{K_{BH^+}}{[H^+]_i + K_{BH^+}}[TB]_i\right),$$

and J_{H^+} is given by Equation 18.

Numerically integrating the above two equations yields the time courses of $[TB]_i$ and $[H^+]_i$, from which we can compute the time-courses of $[BH^+]_i$ and $[B]_i$ from

$$[BH^+]_i = \alpha[TB]_i, \tag{41}$$

$$[B]_i = (1-\alpha)[TB]_i, \tag{42}$$

where

$$\alpha = \frac{[H^+]_i}{[H^+]_i + K_{BH^+}}. \tag{43}$$

Simulation for NH_3/NH_4^+ experiments. BDW employed Equation 39 and Equation 40 to simulate the experiments in which they exposed a squid giant axon to equilibrated NH_3/NH_4^+. Their simulation protocol was a step change in extracellular NH_4Cl from 0 to 9 mM (that is, a step change in $[NH_4^+]_o$ from 0 to 8.86 mM, and in $[NH_3]_i$ from 0 to 0.14 mM) applied for 1500 s (25 min) at constant $pH_o = 7.70$.[10]

Table 1 and Table 3 report the parameter values used by BDW. Note that in the NH_3/NH_4^+ simulations, k is always zero, that is, J_{H^+} does not affect these processes.

The differential Equation 39 and Equation 40 — when coded in CellML and solved with OpenCOR — produce the plots in Figure 6. The simulation file Boron-NH3.sedml contains the computational setting for running the model. Open the .sedml file in OpenCOR and click Run Simulation. The initial conditions are $[TB]_i = 0$ mM and $pH_i = 7.32$.

[10] BDW arrived at the value $[NH_4^+]_o = 8.86$ mM by rearranging the equilibrium relation outside the cell: $[NH_4^+]_o = [H^+]_o\frac{[TB]_o}{[H^+]_o + K_{NH_4^+}} = 8.86$ mM, when $[TB]_o = 9$ mM, $pH_o = 7.70$, and $K_{NH_4^+} = 3.16 \times 10^{-7}$ mM (or equivalently, pK = 9.50). The extracellular NH_3 concentration can be obtained as $[NH_3]_o = [TB]_o - [NH_4^+]_o = 9 - 8.86 = 0.14$ mM

Table 3. Parameter values for simulations of squid-axon NH_3/NH_4^+ experiments.

Symbol	Name	BDW Value	Unit	New Value	Unit
$\beta_{NH_4^+}$	buffering power	−9	mM	9	mM
$[TB]_o$	extracellular total ammonia	9 [1]	mM		
$[NH_3]_o$	extracellular NH_3	0.1404	mM		
$[NH_4^+]_o$	extracellular NH_4^+	8.8596	mM		
P_{NH_3}	membrane permeability	6×10^{-3}	$cm \cdot s^{-1}$	6×10^{-5}	$m \cdot s^{-1}$
$P_{NH_4^+}$	membrane permeability	$0 - 1 \times 10^{-4}$ [2]	$cm \cdot s^{-1}$	1×10^{-6}	$m \cdot s^{-1}$
$K_{NH_4^+}$	acid dissociation constant	0.31623×10^{-6}	mM		
$pK_{NH_4^+}$	acid dissociation constant	9.5			
V_m	membrane potential	−55 [3]	mV	−0.055	V
k	H^+ pump rate constant	0	s^{-1}		
pH_i	intracellular pH	7.32 [4]			

[1] In their original Fortran code that generated the plots in their figure 6B, BDW used $[TB]_o$ = 9 mM (the value used in some of their early experiments), and not 10 mM as (the value used in their later experiments) indicated in the figure and legend for figure 6B in their original paper.

[2] In figure 6B of the BDW paper, $P_{NH_4^+}$ had values of 0, 10^{-6}, 10^{-5}, and 10^{-4} cm^{-1}.

[3] BDW did not report the value of V_m, but in their code used *−55* mV, which matched the measured mean value.

[4] In their code BDW used the value of 7.32 and not 7.30, which they used when constructing the Davenport diagram in their figure 5B.

5 Discussion

The publication of this retrospective paper provides an opportunity to clarify some concepts in the original paper that have benefitted from subsequent experimental and theoretical advances. We also provide some additional parameters missing from BDW and correct some minor errors. Most importantly, the curated model is now freely available on the Physiome website[11] in standardised form (CellML) that can be run in the open source software OpenCOR. A follow-up paper will be written that recasts the equations in bond graph form to facilitate their incorporation into more complex models where pH regulation is coupled with other cellular processes.

5.1 Historical Context

The 1976 Boron & De Weer paper introduced the first models to simulate the time course of pH_i. By developing a predictive mathematical model based on first principles, BDW provided a quantitative basis for interpreting their new data on the time-dependent response of pH_i to step changes in extracellular CO_2/HCO_3^- (and HA/A^- pairs in general) and NH_3/NH_4^+ (and B/BH^+ pairs in general). The models also provided a clear, quantitative basis for interpreting BDW's new data on how cells regulate their pH_i, which BDW modelled as a pH_i-dependent H^+-extrusion mechanism. Below, we will introduce a broader concept termed "acid extrusion" (Boron, 1977). The first of the two BDW models elucidates how the transmembrane fluxes of a neutral weak acid and its anionic conjugate weak base affects pH_i, with the acid-extrusion becoming increasingly important as pH_i falls. The second model simulates how the transmembrane fluxes of a neutral base and its cationic conjugate weak acid affects pH_i.

[11] https://models.physiomeproject.org/workspace/5f8

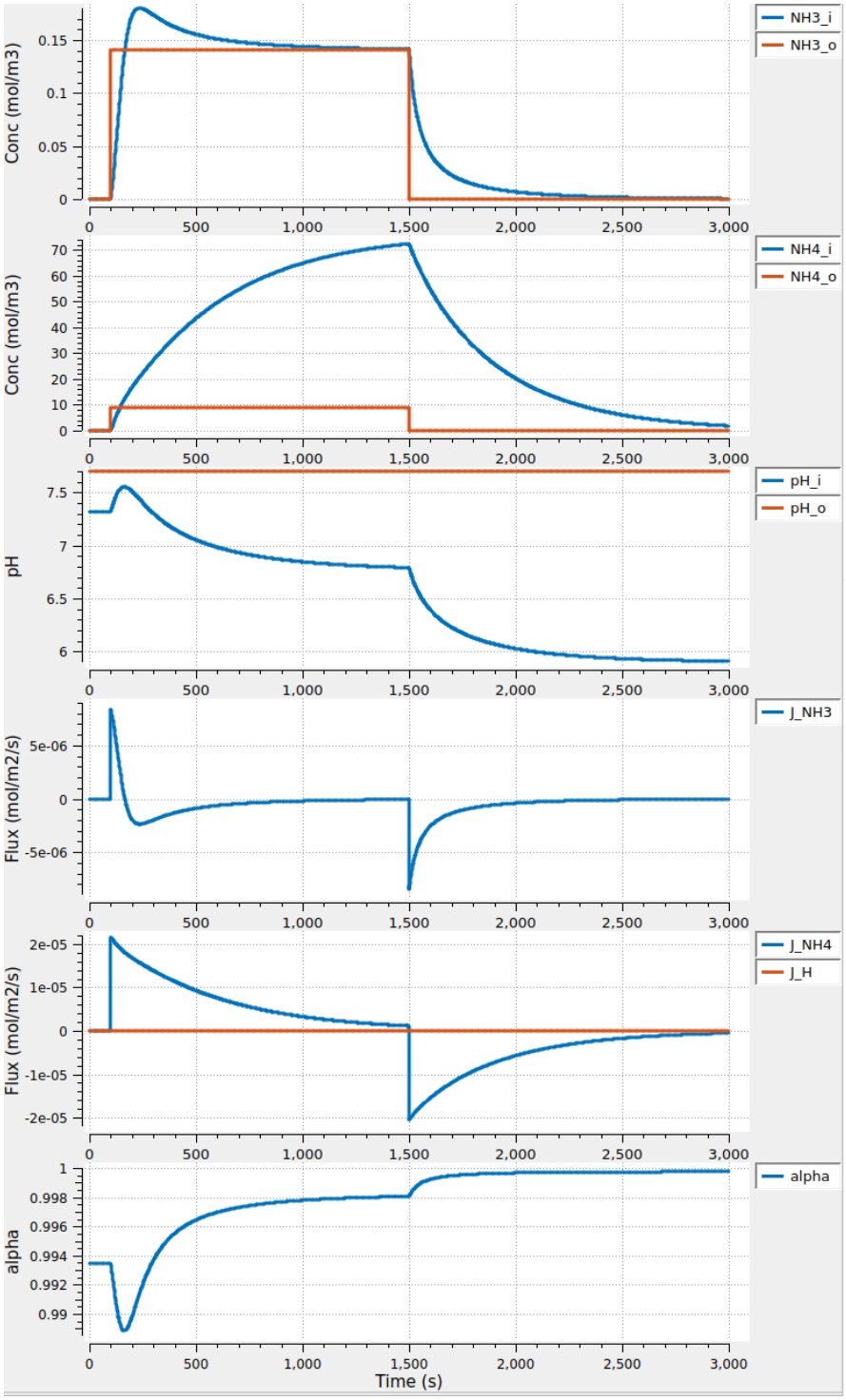

Figure 6. Solution of the BDW model during and following a 1500 s period of externally applied NH_4Cl. In these simulations $[NH_4^+]_o$ = 9 mM. The intracellular fluid becomes alkaline as NH_3 enters (note the J_{NH_3} time course) and hydrates to form NH_4^+ and OH^-. Additional passive NH_4^+ entry (note $J_{NH_4^+}$ time course) down its electrochemical gradient opposes the effect of the NH_3 entry and slightly reduces the pH_i increase. Upon removal of NH_4Cl, $[NH_3]_i$ and $[NH_4^+]_i$ decay towards their original values, but pH_i drops well below its original value of 7.40.

Of course, BDW were not the first to undertake a quantitative assessment of how acids or bases

affect, or are affected by, the pH of a solution. Below, we divide the earlier work into two major categories, (a) analyses of how neutral weak acids (and their anion conjugate weak bases) or neutral weak bases (and their cationic conjugate weak acids) affect pH in simple systems, and (b) analyses of how the distribution of HA/A^- (or B/BH^+) across a barrier, such as a cell membrane, are affected by pH_i and V_m.

5.2 Development of the Concept of Buffering in Simple and Complex Systems

Buffering power. In 1914, Koppel (1914) introduced the first modern definition of the chemical buffering (*i.e.*, "magnitude of moderation", or P) of H^+ by a weak-acid/weak-base conjugate pair, and — based on first principles — derived an expression for buffering power. Because these authors defined P in terms of the amount of strong acid that one must add to a solution to produce a pH change, P is a negative number. Roos and Boron (1980) translated the Koppel-Spiro paper from its original German, and provided a historical context.

Initially unaware of the work of Koppel and Spiro, Van Slyke (1922) independently defined buffering power — to which he assigned the Greek letter β. Because he defined β in terms of the amount of strong base that one must add to a solution to produce a pH change (see Equation 8), β is a positive number. Although modest differences exist between the efforts of Koppel and Spiro on the one hand and Van Slyke on the other, they are quite similar. Nevertheless, it is Van Slyke's definition of β that has become the modern convention throughout chemistry and physiological chemistry.

Koppel & Spiro and Van Slyke quantitatively described how — in a one-compartment solution — weak acids, weak bases, ampholytes, and weak-acid/base mixtures can buffer added strong acid or strong base. In their analysis, the system both begins and ends in an equilibrium state. Of course, in their pioneering work, these authors had no reason to contemplate time courses or barriers separating more than one compartment.

In their work, BDW defined β as a negative number, as Koppel and Spiro defined their P.

The "Davenport" diagram. This nomogram (Boron and Boulpaep, 2016) is a powerful tool for graphically computing the effects of respiratory acid-base disorders (caused by changes in $[CO_2]$ in a system open to CO_2) and metabolic acid-base disorders (caused by the addition or removal of HCO_3^- or a strong acid or base). The underlying assumption for the Davenport diagram is that the system is in equilibrium. The first component of a Davenport diagram (see Figure 7) is a plot of $[HCO_3^-]$ vs pH_i for one or more values of $[CO_2]$ — these are the CO_2 isopleths that describe the equilibrium among CO_2, HCO_3^-, and H^+. At any pH on any isopleth, the slope is the open-system CO_2/HCO_3^- buffering power (β_{CO_2}). The second component is a linear plot, on the same axes, of the concentration of all protonated forms of all non-HCO_3^- buffers vs pH. At any pH, the slope is the buffering power of all non-HCO_3^- buffers ($\beta_{non-HCO_3^-}$), and the line is termed the non-HCO_3^- buffer line. Its linearity implies that $\beta_{non-HCO_3^-}$ is insensitive to changes in pH. The intersection of an isopleth with the non-HCO_3^- buffer line describes the current state of the system, when both CO_2/HCO_3^- buffer and non-HCO_3^- buffers are simultaneously in equilibrium. Davenport developed a series of rules for using this paradigm to interpret acid-base disorders, and these rules are well founded in physical chemistry.

The Davenport diagram traces its origins to the analyses of blood by several eminent investigators about a century ago. It was Henderson (1921) — as far as we are able to ascertain — who in figure 4 of his paper was the first to plot $[HCO_3^-]$ vs pH for two H_2CO_3 (rather than CO_2) isopleths, and for two different values of $\beta_{non-HCO_3^-}$ (*i.e.*, those produced by 10% and 100% HbO_2).

The power of the Davenport approach is that, knowing the initial conditions and the pH dependence of $\beta_{non-HCO_3^-}$, one can compute with fair accuracy (using the nomogram) or great accuracy (using a computer to solve the equations numerically) the result of virtually any acid-base disorder in the pathophysiological range for a system containing CO_2/HCO_3^- and a mixture of non-HCO_3^- buffers. In their figure 5A (reproduced here as Figure 7), BDW used a Davenport approach to describe the initial steady state of a squid giant axon (point A at $pH_i \approx 7.32$, $[CO_2]_i = 0.1\%$), the initial effect of an exposure to increased $[CO_2]_i$ (point B, an example of intracellular respiratory

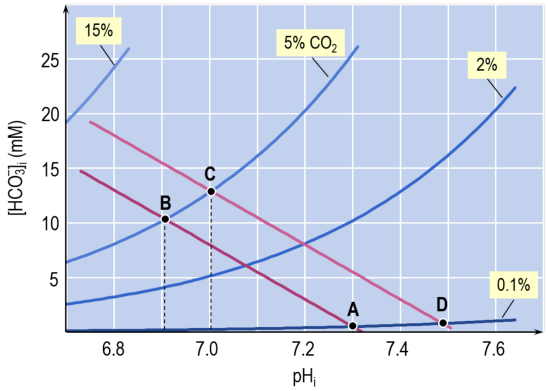

Figure 7. A Davenport diagram (from figure 5A of BDW). This nomogram consists of two kinds of plots. The first kind of plot is represented by the four CO_2 isopleths that slope upwards from left to right. Each isolpleth represents all possible combinations of $[HCO_3^-]_i$ and pH_i for a given $[CO_2]_i$ (described here as the % of the air phase that is CO_2). The second kind of plot is represented by the two lines that slope downwards from left to right. The slope of these parallel lines describes the buffering power of non-CO_2/HCO_3^- buffers. BDW assumed that the experiment starts at point A, at pH_i = 7.32 and 0.1% CO_2. The addition of 5% CO_2 causes the pH_i at equilibrium to fall to the point represented by point B. The extrusion of acid during the CO_2/HCO_3^- exposure causes the system to move along the 5% CO_2 isopleth from point B to point C. Finally, upon removal of CO_2/HCO_3^-, the system returns to the original CO_2/HCO_3^- isopleth, but now at point D. The difference between points D and A represents the pH_i overshoot. In the BDW paper, β — the slope of the lines in this figure — appeared to be 25 mM/pH unit. In fact, the value of β determined in the NH_3/NH_4^+ experiments (also shown as a Davenport-like diagram in figure 5B of BDW) was 9 mM/pH unit. The reason for this discrepancy was probably that BDW delivered the CO_2/HCO_3^- solution to the axon using a peristaltic pump and Silastic tubing, which they later realised has a high CO_2 permeability. Thus, the $[CO_2]$ reaching the axon was < 5%, accounting for the artificially inflated value for β. In their follow-up paper (Boron and De Weer, 1976), BDW delivered the CO_2/HCO_3^- solutions from glass syringes and through Saran tubing, which has an extremely low CO_2 permeability.

acidosis), the effect of the plateau-phase pH_i recovery (point C, an example of intracellular compensatory metabolic alkalosis), and finally the effect of removing extracellular CO_2 (point D, an example of metabolic alkalosis) to account for the pH_i overshoot. If one does not know $\beta_{non-HCO_3^-}$, the Davenport diagram allows one to compute it from the initial and final pH . The numerical integration of the BDW equations — when $P_{HCO_3^-}$ and the acid extrusion rate are both zero — should in principle yield, at infinite time, results consistent with the Davenport diagram.

In their paper (their figure 5B), BDW introduced a novel Davenport-like diagram for the NH_3/NH_4^+ buffer system, with $[NH_4^+]$ on the ordinate (replacing $[HCO_3^-]$), NH_3 isopleths (replacing CO_2 isopleths), and a line describing non-NH_3/NH_4^+ buffering power (replacing the line describing non-CO_2/HCO_3^- buffering power). Like the classical Davenport diagram, this one (or others like it, constructed for other buffer pairs) can be a useful tool for interpreting — in the steady state — problems in acid-base chemistry.

In the Davenport analysis, the initial and final conditions represent equilibria. Davenport-like diagrams provides no information about the time course of pH between the initial and final states. Nor can Davenport-like diagrams deal with time course, barriers (*e.g.*, cell membranes), permeabilities to substances other than the neutral molecule (*e.g.*, CO_2, NH_3), or active transport. Of course, in their pioneering work, Henderson, Davenport, and other authors contributing to this nomogram had no reason to contemplate these future complexities.

5.3 Pre-BDW Analyses of Transmembrane Distributions of Weak Acids and Bases

As summarised by Roos and Boron (1981), about a century ago, several authors — who assumed that CO_2 equilibrates across the plasma membrane but that HCO_3^- is impermeant — used the sum $[CO_2]_i + [HCO_3^-]_i$ to compute the steady-state pH_i of several cell types. Then, beginning in 1940, a series of authors introduced three successively more sophisticated mathematical analyses for the steady-state transmembrane distribution of a neutral weak acid and its anionic conjugate weak base (*i.e.*, TA), and three more for the distribution of a neutral weak base and its cationic, conjugate weak acid (*i.e.*, TB). We will now present these analyses in order of increasing complexity, and according to their sequence in time (see Figure 8). They all have in common the assumption that the system is either in equilibrium or at least in a steady state supported by the input of energy.

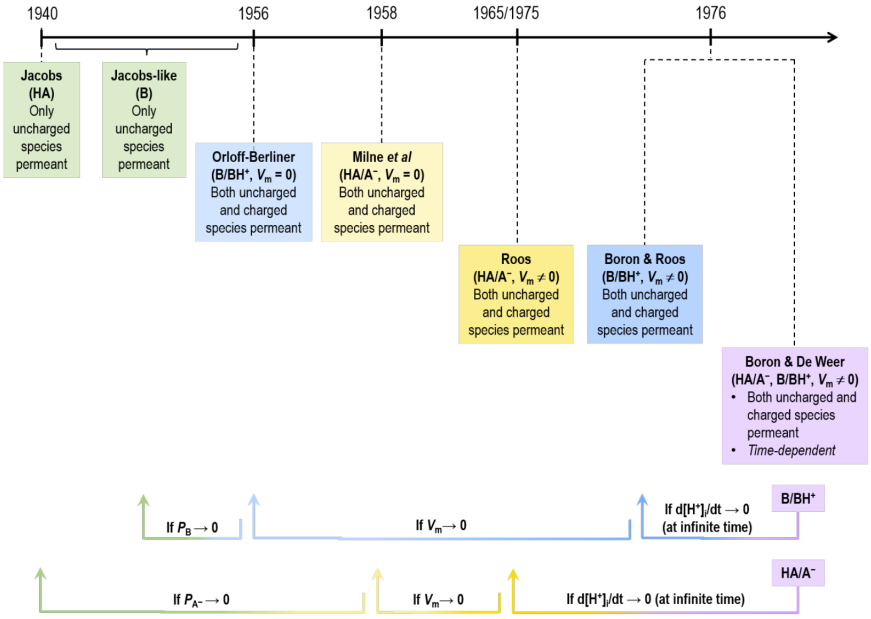

Figure 8. Timeline of acid-base/pH models prior to BDW. Note that the time-dependent BDW model of weak acid/conjugate weak base (HA/A^-) collapses to Roos (1965, 1975) steady-state model for HA/A^-. The Roos (1965, 1975) model, in turn, reduces to the Milne et al. (1958) model for HA/A^- when the membrane potential (V_m) approaches zero. Finally, the Milne et al. (1958) model reduces to the Jacobs (1940) model — where only one uncharged species HA is permeant — as the permeability of A^- (P_{A^-}) approaches zero. Similarly, the time-dependent BDW model of weak base/conjugate weak acid (B/BH^+) collapses to Boron and Roos (1976) steady-state model for B/BH^+. The Boron and Roos (1976) model in turn reduces to the Orloff and Berliner (1956) model for B/BH^+ when V_m approaches zero. Finally, the Orloff and Berliner (1956) model reduces to the Jacobs-like model — where only one uncharged species B is permeant — as (P_B) approaches zero.

Jacobs (HA, neutral weak acid). Jacobs (1940) presented a general mathematical model that describes the equilibrium transmembrane distribution of total weak acid (TA), assuming that only the neutral species (HA), but not the conjugate weak base (A^-) can cross the membrane:

$$\frac{[TA]_i}{[TA]_o} = \frac{10^{pH_i - pK} + 1}{10^{pH_o - pK} + 1}. \tag{44}$$

In an accompanying document, we show the derivation of the above equation[12], the linear form of which is:

$$\frac{[TA]_i}{[TA]_o} = \left(\frac{[H^+]_i + K}{[H^+]_o + K}\right)\left(\frac{[H^+]_o}{[H^+]_i}\right). \tag{45}$$

[12] See equation 24 in Derivation of the Jacobs Neutral Weak Acid Equation (Log) in Supplementary Files

We also present the derivation of this linear version in an accompanying document[13]. A major assumption in the derivations of both Equation 44 and Equation 45 is that HA does not merely move but fully equilibrates across the cell membrane. That is, the system is in equilibrium.

The notion that only the neutral member of the buffer species (*i.e.*, HA) can traverse the membrane is known as nonionic diffusion. Equation 44 and Equation 45 tell us that, as pH_i rises (*i.e.*, $[H^+]_i$ falls), $[TA]_i$ rises steeply because $[A^-]_i$ rises exponentially with pH_i — a concept known as "trapping" (of the A^-).

Jacobs-like equation (B, neutral weak base). Although Jacobs did not present the analogous equation for total weak base (TB), others have derived it, including Roos and Boron (1981):

$$\frac{[TB]_i}{[TB]_o} = \frac{10^{pK-pH_i} + 1}{10^{pK-pH_o} + 1}. \tag{46}$$

In an accompanying document, we show the derivation of Equation 46,[14] the linear form of which is:

$$\frac{[TB]_i}{[TB]_o} = \frac{[H^+]_i + K}{[H^+]_o + K}. \tag{47}$$

We also present a derivation of Equation 47.[15] A major assumption in the derivations of Equation 46 and Equation 47 — analogous to the situation for Equation 44 and Equation 45 — is that B fully equilibrates across the cell membrane. That is, the system is in equilibrium.

The notion that only the neutral member of the buffer species (*i.e.*, B) can traverse the membrane is another example of nonionic diffusion. Equation 46 and Equation 47 tell us that, as pH_i falls (*i.e.*, $[H^+]_i$ rises), $[TB]_i$ rises steeply because $[BH^+]_i$ rises exponentially with the decrease in pH_i — another example of "trapping" (of the BH^+). Such trapping is especially important in renal physiology, where acidic fluid in renal tubules can trap the cationic form of a buffer pair (*e.g.*, NH_4^+).

Equation 44 and Equation 46 provide the theoretical foundation for using $[TA]_i/[TA]_o$ ratios for permeant weak acids (*e.g.*, CO_2, above, and the later 5,5'-dimethyl-2,4-oxazolidinedione [DMO] technique) or $[TB]_i/[TB]_o$ ratios for permeant weak bases (*e.g.*, for methylamine; see Boron and Roos (1976)) for computing steady-state pH_i. For example, equation tells us that, as pH_i rises, $[TA]_i/[TA]_o$ will rise nearly exponentially; this occurs because $[A^-]_i$ rises in a precisely exponential fashion.

Orloff & Berliner (B/BH^+, $V_m = 0$). Orloff and Berliner (1956) extended the Jacobs-like model to a neutral weak base and its cationic conjugate weak acid by permitting not just B but also BH^+ to permeate a barrier separating compartments 1 and 2. They avoided the complication of BH^+ electrodiffusion by assuming a transmembrane voltage of zero (*i.e.*, $V_m = 0$). Because they recognised that the flux of BH^+ across the barrier would cause pH to drift in opposite directions in the two compartments, they assumed that independent, energy-requiring processes would stabilise pH in the two compartments and establish a steady state described by

$$\frac{P_B}{P_{BH^+}} = \frac{[BH^+]_i - [BH^+]_o}{[B]_o - [B]_i}. \tag{48}$$

In an accompanying document[16], we show the derivation of Equation 48. If we put Equation 48 into the same form as Equation 47, which expresses the buffer concentrations in terms of $[TB]_i$ and $[TB]_o$ then — for cells — we have

$$\frac{[TB]_i}{[TB]_o} = \left(\frac{[H^+]_i + K}{[H^+]_o + K}\right)\left(\frac{\frac{P_B}{P_{BH^+}}K + [H^+]_o}{\frac{P_B}{P_{BH^+}}K + [H^+]_i}\right). \tag{49}$$

[13] See equation 25 in Derivation of the Jacobs Neutral Weak Acid Equation (Linear) in Supplementary Files
[14] See equation 33 in Derivation of a Jacobs-like Equation (Log) for a Neutral Weak Base in Supplementary Files
[15] See equation 21 in Derivation of a Jacobs-like Equation (Linear) for a Neutral Weak Base in Supplementary Files
[16] See equation 26 in Derivation of the Orloff-Berliner Equation in Supplementary Files

As P_{BH^+} approaches zero, Equation 49 reduces to Equation 47 — the Jacobs-like equation for a weak base. The accompanying document[17] also shows the derivation of Equation 49, as well as the mathematics that shows the limit of this expression as P_{BH^+} approaches zero.

Note that the flux of BH^+ — which leads to a flux of B in the opposite direction — tends to push the system off equilibrium. As noted above, the Orloff-Berliner equation requires that the system be in a steady-state, which can be achieved, as they recognised, only by an input of energy to maintain all relevant concentrations constant over time.

Milne et al (HA/A^-, $V_m = 0$). Milne and colleagues (1958) developed a steady-state expression similar to that of Orloff & Berliner, but for the transmembrane distribution of a neutral weak acid and its anionic conjugate weak:

$$\frac{P_{HA}}{P_{A^-}} = \frac{[A^-]_i - [A^-]_o}{[HA]_o - [HA]_i}. \tag{50}$$

An accompanying document[18] shows the derivation of Equation 50, which we can also put in the form of Equation 49, which expresses buffer concentrations in terms of $[TA]_i$ and $[TA]_o$:

$$\frac{[TA]_i}{[TA]_o} = \left(\frac{[H^+]_i + K}{[H^+]_o + K}\right)\left(\frac{\frac{P_{HA}}{P_{A^-}}[H^+]_o + K}{\frac{P_{HA}}{P_{A^-}}[H^+]_i + K}\right). \tag{51}$$

As P_{A^-} approaches zero, Equation 51 reduces to Equation 45 — the Jacobs equation for a weak acid. The accompanying document[19] also shows the derivation of Equation 51, as well as the mathematics that shows the limit of this expression as P_{A^-} approaches zero.

Roos (HA/A^-, non-zero V_m). In 1965 and 1975, Roos extended the Irvine model by allowing V_m to assume non-zero values (Roos, 1965, 1975), and derived the following equation,

$$\frac{[TA]_i}{[TA]_o} = \left(\frac{[H^+]_i + K}{[H^+]_o + K}\right)\left(\frac{\frac{P_{HA}}{P_{A^-}}[H^+]_o + \frac{FV_m}{RT(1-\epsilon)}K}{\frac{P_{HA}}{P_{A^-}}[H^+]_i + \frac{FV_m}{RT(1-\epsilon)}K}\right), \tag{52}$$

where ϵ has the same meaning as in the derivation of the BDW equations: $e^{-V_m F/RT}$. An accompanying document[20] shows the derivation of Equation 52. This document also shows that, at the limits of certain parameters, Equation 52 simplifies to the expected equation:

1. As $V_m \to 0$, the Roos equation simplifies to the equation of Milne et al (which assumes $V_m = 0$).
2. As $P_{A^-} \to 0$, the Roos equation simplifies to the Jacobs equation (which assumes $P_{A^-} = 0$).
3. As $P_{HA} \to 0$, the Roos equation simplifies to the Nernst equation (which assumes permeability to only A^-).

The Roos equation was important historically because it allowed one to assess possible errors in pH_i values computed from the transmembrane distribution of a neutral weak acid (*e.g.*, CO_2, DMO) and its monovalent anion conjugate weak base. These errors could in principle arise from membrane permeability to A^- (as already considered by Milne et al), as influenced by V_m.

Boron & Roos (B/BH^+, non-zero V_m). Finally, Boron and Roos (1976) derived an equation similar to the Roos equation, but for the distribution of a neutral weak base and its monovalent cationic

[17] See equation 55 in Derivation of the Orloff-Berliner Equation in Supplementary Files
[18] See equation 26 in Derivation of the Equation of Milne et al for a Neutral Weak Acid in Supplementary Files
[19] See equation 62 in Derivation of the Equation of Milne et al for a Neutral Weak Acid in Supplementary Files
[20] See equation 45 in Derivation of the Roos Equation in Supplementary Files

conjugate weak acid:

$$\frac{[TB]_i}{[TB]_o} = \left(\frac{[H^+]_i + K}{[H^+]_o + K}\right)\left(\frac{\frac{P_B}{P_{BH^+}}K + \frac{FV_m}{RT(\epsilon' - 1)}[H^+]_o}{\frac{P_B}{P_{BH^+}}K + \frac{FV_m}{RT(\epsilon' - 1)}\epsilon'[H^+]_i}\right), \tag{53}$$

where ϵ' has the same meaning as in the derivation of the BDW equations: $e^{V_m F/RT}$. An accompanying document[21] shows the derivation of Equation 53. This document also shows that, at the limits of certain parameters, Equation 53 simplifies to the expected equation:

1. As $V_m \rightarrow 0$, the Boron-Roos equation simplifies to the equation of Orloff & Berliner (which assumes $V_m = 0$).
2. As $P_{BH^+} \rightarrow 0$, the Boron-Roos equation simplifies to the Jacobs-like equation for a neutral weak base (which assumes $P_{BH^+} = 0$).
3. As $P_B = 0$, the Boron-Roos equation simplifies to the Nernst equation (which assumes permeability to only BH^+).

The Boron-Roos equation was important historically because it allowed one to assess possible errors in pH_i values computed from the transmembrane distribution of a neutral weak base (*e.g.*, methylamine) and its monovalent anion conjugate weak base. These errors could in principle arise from membrane permeability to BH^+, as influenced by V_m. In their paper, Boron and Roos used the transmembrane distribution of methylamine/methylammonium to monitor a downward drift in pH_i caused by the passive influx of methylammonium. This was the first use of a chemical-distribution technique to follow pH_i changes over time.

We have already noted for the Orloff-Berliner equation that the derivation requires that the system be in a steady-state, which can be achieved only by an input of energy to maintain all relevant concentrations constant over time. The same is true for the equations of Milne et al, Roos, and Boron & Roos.

5.4 Comparison of the Pre-BDW Analyses with the BDW Equations

The BDW equations build on the earlier work on buffering and transmembrane distributions of weak acids and bases, presented in the previous two sections. Of course, the work of Koppel and Spiro, and Van Slyke, as well as their predecessors who developed the physico-chemical principles of acid-base chemistry, is at the heart of the BDW model.

An important aspect of the Davenport diagram is its predictive power. For example, given $\beta_{non-HCO_3^-}$ as well as the initial pH and $[CO_2]$, the Davenport approach can predict the effect of an increase in $[CO_2]$ on the final equilibrium conditions. However, the Davenport approach makes no statement about mechanism or time course. The BDW approach has all the predictive power of Davenport, but also addresses mechanism and time course.

The six pre-BDW approaches for assessing transmembrane distributions of HA/A^- and B/BH^+ all start with the weak acid/base present and the system in an equilibrium or at least in a steady state. Somehow, the system — the cell and its surrounding fluid — went from a condition with no weak acid/base present to a condition with the weak acid/base present at equilibrium/steady state. The older models make no attempt to describe how and how fast the system achieved the new state, and — unlike the Davenport approach — have no predictive value for relating initial and final conditions. It is worth noting that the investigators who developed these six approaches were interested mainly in using tracer levels of weak acids/bases to compute pH_i. The intention was that tracer levels would have minimal effects on the state of the system — hence, the minimal interest in the prediction. Note that, at infinite time (and with no acid extrusion), the BDW equations reduce to those six transmembrane-distribution analyses presented in the previous section.

To some extent, the BDW models represent a merger of the Davenport and the six pre-BDW approaches for assessing transmembrane distributions of HA/A^- and B/BH^+. Like the Davenport

[21] See equation 44 in Derivation of the Boron-Roos Equation in Supplementary Files

approach, the BDW approach is predictive. However, unlike Davenport's approach, the BDW models provide insight into mechanism and time course, and are applicable even when the system is far from equilibrium/steady state. Like the six transmembrane-distribution models, the BDW models provide insight into how pH_i and V_m affect $[HA]_i$, $[A^-]_i$, $[B]_i$, and $[BH^+]_i$. Unlike the six transmembrane-distribution models, the BDW models are predictive and provide insight into mechanism and time course.

It is worth noting that BDW derived their equations under the influence of Albert Roos, who had derived the transmembrane-distribution model for HA/A^- (Roos, 1975) and who inspired Boron's derivation of the B/BH^+ model (Boron and Roos, 1976).

5.5 Post-BDW Development of Concepts

Fundamental law of pH_i regulation. Recall that one of the intermediate steps of the derivation of the BDW equations for the HA/A^- system was Equation 21, which we reproduce here:

$$\frac{dpH}{dt} = \left(\frac{-1}{\beta}\right)\left(\frac{dQ}{dt}\right). \tag{54}$$

Another intermediate step was the description of dQ/dt in Equation 17, which we reproduce here:

$$\frac{dQ}{dt} = \rho\Big((1-\alpha)J_{HA} - \alpha J_{A^-} - J_{H^+}\Big). \tag{55}$$

Combining the above two equations yields a primitive form of the fundamental law of pH_i regulation:

$$\frac{dpH_i}{dt} = -\frac{1}{\beta}\underbrace{\rho\Big((1-\alpha)J_{HA} - \alpha J_{A^-} - J_{H^+}\Big)}_{dQ/dt}. \tag{56}$$

In the later literature, Boron and colleagues in effect dissected the dQ/dt term — the net rate at which H^+ appear in the cytosol ($mol \cdot m^{-3} \cdot s^{-1}$) — into two concepts that are more general than those considered by BDW in Equation 56: the intracellular acid-loading rate (J_L) and the intracellular acid-extrusion rate (J_E).

In the narrow definition of Equation 56 the only J_L term is $(1-\alpha)J_{HA}$. In the post-BDW literature, Boron and colleagues defined J_L to comprise every process that adds the equivalent of H^+ to or removes the equivalent of OH^- from the cytosol, including H^+ channels (mediating passive H^+ influx), a variety of transporters (*e.g.*, Cl-HCO_3 exchangers mediating HCO_3^- efflux), and the metabolic production of acid. Boron et al. (1979) measured and introduced the term "rate of acid introduction". Roos and Boron (1981) later replaced this term when they coined "acid-loading rate".

In the narrow definition of Equation 56, the J_E terms are αJ_{A^-} and J_{H^+}. Note that BDW defined J_{H^+} as the H^+-extrusion rate above baseline. In the post-BDW literature, Boron and colleagues defined J_E to comprise every process that removes the equivalent of H^+ from or adds the equivalent of OH^- to the cytosol, including a variety of transporters (*e.g.*, H^+ pumps, Na-H exchangers) that mediate H^+ efflux and others (*e.g.*, Na^+-driven HCO_3^- transporters, H^+/lactate cotransporters) that mediate base efflux. It appears that Boron in 1977 provided the first definition of acid extrusion.

Recasting Equation 56 in terms of J_L and J_E,

$$\frac{dpH_i}{dt} = -\frac{1}{\beta}\underbrace{\rho\Big(\underbrace{(1-\alpha)J_{HA}}_{J_L\text{ term}}\underbrace{-\alpha J_{A^-} - J_{H^+}}_{J_E\text{ terms}}\Big)}_{dQ/dt}. \tag{57}$$

The modern version of the fundamental law of pH_i regulation is:

$$\frac{dpH_i}{dt} = \frac{\rho}{\beta}(J_E - J_L). \tag{58}$$

Here, with the explicit inclusion of ρ, J_E and J_L have the units (moles $\cdot$ cm^{-2} $\cdot$ s^{-1}).

Equation 58 tells us that pH_i is stable when $J_E = J_L$, rises when $J_E > J_L$, and falls with $J_E < J_L$. BDW did not derive the above equation in their 1976 paper. The first statement of the concept of Equation 58 was in sentence form in the review by Roos and Boron (1981), who also provided a graphical example in their figure 12. By 1989, Boron presented a version of Equation 58 that lacks the term ρ. Thus, he implicitly defined J_E and J_L in terms of (moles $\cdot$ cm^{-3} $\cdot$ s^{-1}). This 1989 paper also included examples of how Equation 58 could help one interpret the time course of pH_i in many experimental settings. For example, a bolus introduction of acid into a cell — an "acute" intracellular acid load, coined by Boron by the time of this 1989 review — rapidly lowers pH_i, but also increases J_E and decreases J_L. Because J_E now exceeds J_L, pH_i recovers to its initial value. By 1992, Boron coined the term "fundamental law of pH_i regulation" to describe Equation 58.

Note that an acute or bolus intracellular acid load is to be distinguished from a chronic intracellular load (the rate of which is J_L). The amount of an acute acid load can instantly be quantitated in acid equivalents. The amount of a chronic acid load can only be quantitated in acid equivalents by integrating J_L over time.

Later, Boron (2004) provided a more detailed description of pH_i regulation, as well as a tongue-in-cheek analogy — which he had been using for years in lectures — between pH_i regulation and the temperature regulation of a house, complete with multiple furnaces (acid-extruders), multiple air conditioners (acid loaders), heat capacity (buffering power), a thermostat (pH_i sensitivity of the transporters), and weather radar (extracellular sensors for CO_2, HCO_3^-, and pH).

Flux vs pseudoflux. One can define the acid-loading and acid-extrusion rates as strict fluxes, with units of moles/(membrane area $\times$ time). Such of use of J_E or J_L — for example J_{NBC} (the acid-extruding flux mediated by a Na/HCO_3 cotransporter, NBC) or J_{Cl-HCO_3} (the acid-loading flux mediated by a Cl-HCO_3 exchanger) — is most appropriate in cases in which the cell has a simple geometry (*e.g.*, a squid axon or *Xenopus* oocyte). However, for cells with complex geometries — where surface-to-volume ratios are difficult to define — physiologists often present experimental data in the units "moles/(volume of cell water)". To avoid confusion between the two systems of measurement, Bevensee and Boron (1995) introduce the term "pseudoflux" and the symbol ϕ (rather than J). Thus, in their paper, the authors referred to ϕ_E and ϕ_L (rather than J_E and J_L), so that the fundamental law of pH_i regulation becomes

$$\frac{dpH_i}{dt} = \frac{\phi_E - \phi_L}{\beta}. \tag{59}$$

Effect of isodirectional fluxes of HA/A^- or B/BH^+ fluxes on pH near a membrane. The α term in Equation 14 and Equation 37, and the $(1-\alpha)$ term in Equation 16 and Equation 38 inspired an insight that yields equations analogous to the familiar Henderson-Hasselbalch equation. The starting point was the following question: if both B and BH^+ cross the membrane in the same direction, how will their isodirectional fluxes affect pH on the *cis* side (the side from which they depart) and the *trans* side (the side to which they go)?

In the discussion of their paper, Musa-Aziz et al. (2009b) showed that if the flux ratio $J_{NH_3}/J_{NH_4^+}$ is the same as the concentration ratio $[NH_3]_i/[NH_4^+]_i$, the flux will have no effect on pH_i because NH_3 and NH_4^+ are appearing (or disappearing) at the inner surface of the membrane in a proportion equal to their respective, pre-existing concentrations. Similarly, if the flux ratio $J_{NH_3}/J_{NH_4^+}$ is the same as the concentration ratio $[NH_3]_o/[NH_4^+]_o$, the flux will have no effect on pH_o. Stated somewhat differently, as in equation 4 of Musa-Aziz et al. (2009b),

$$pH_{i,Null} = pK_a + \log\frac{J_{NH_3}}{J_{NH_4^+}}, \quad \text{or more generally,} \quad pH_{i,Null} = pK_a + \log\frac{J_B}{J_{BH^+}} \tag{60}$$

and

$$pH_{o,Null} = pK_a + \log \frac{J_{NH_3}}{J_{NH_4^+}}, \quad \text{or more generally,} \quad pH_{o,Null} = pK_a + \log \frac{J_B}{J_{BH^+}} \tag{61}$$

Here, $pH_{i,Null}$ is the pH_i at which the isodirectional fluxes J_B and J_{BH^+} will have no effect on pH_i. Similarly, $pH_{o,Null}$ is the pH_o at which the isodirectional fluxes J_B and J_{BH^+} will have no effect on pH_o. If $pH_i = pH_o$, then their null pH values are the same (*i.e.*, at this pH, the isodirectional fluxes of B and BH^+ will have no effect on either pH). One can write equations similar to Equation 60 and Equation 61, but for CO_2 and HCO_3^- (or HA and A^-), which we do here for the first time:

$$pH_{i,Null} = pK_a + \log \frac{J_{HCO_3^-}}{J_{CO_2}}, \quad \text{or more generally,} \quad pH_{i,Null} = pK_a + \log \frac{J_{A^-}}{J_{HA}} \tag{62}$$

and

$$pH_{o,Null} = pK_a + \log \frac{J_{HCO_3^-}}{J_{CO_2}}, \quad \text{or more generally,} \quad pH_{o,Null} = pK_a + \log \frac{J_{A^-}}{J_{HA}} \tag{63}$$

The previous four equations can be valuable for interpreting, for example, the effects of isodirectional fluxes of CO_2 and HCO_3^-. The equations cannot predict the speed or extent of the pH change, only the direction. For instance, if we expose a cell to a CO_2/HCO_3^- solution and pH_i falls, does mean that $J_{CO_2} > J_{HCO_3^-}$? The intuitive answer would be, "yes". The actual answer is, "not necessarily". Imagine that — in a CO_2/HCO_3^--free environment — we have a CO_2/HCO_3^--free cell at a pH_i of 7.1. Although no CO_2/HCO_3^- is present, we assume that the pK_a of the CO_2/HCO_3^- equilibrium would be 6.1 if CO_2/HCO_3^- were present. We now suddenly add CO_2/HCO_3^- to the extracellular fluid — the precise ratio is of no consequence here because we will focus on the intracellular fluid. CO_2 and HCO_3^- now begin to enter the cell by any route. If the ratio $J_{HCO_3^-}/J_{CO_2} = 10^{pH_i - pK_a} = 10^{7.1-6.1} = 10$, then pH_i will not change from its original value of 7.1 because HCO_3^- and CO_2 are entering the cell precisely in the correct ratio for a pH of 7.1. If $J_{HCO_3^-}/J_{CO_2} < 10$ (in this case), pH_i will fall because the alkalinising pH_i effects of the HCO_3^- influx are less than the acidifying pH_i effects of the CO_2 influx. This approach cannot tell us how fast or how far pH_i will fall, only that, initially at least, it must fall. The same analysis can be applied — simultaneously — to the extracellular fluid.

5.6 Post-BDW Models of Acid-Base Fluxes/Chemistry

Following the development of the BDW model, the field of pH regulation has seen several modelling efforts. Here, we summarise several, with emphasis on those models that, in our opinion and to the best of our knowledge, have contributed to advance the field, either by extending the BDW model or by introducing new modelling paradigms.

Keifer and Roos. In 1981, Keifer and Roos refined the BDW model by modifying the BDW assumption that addition of an infinitesimal amount of weak acid HA (or A^-, B, or BH^+) during an infinitesimal increment in time does not alter the pre-existing equilibrium ratio $[HA]_i/[A^-]_i$ or $[B]_i/[BH^+]_i$ (Keifer and Roos, 1981). These authors were interested in the transmembrane fluxes of the neutral weak acid DMO and its conjugate weak base. Keifer & Roos assumed that — at the end of the infinitesimal time increment during which HA and A^- entered/left the cell — the cytosolic HA, A^- and H^+ re-equilibrated. They used this variation on the BDW approach to estimate P_{HA} and P_{A^-}, finding that the plasma membrane permeability to HA is $\approx 10^3$ higher than to A^-. In the appendix of their paper, Keifer & Roos derived their refined version of the BDW equations for HA/A^-:

$$\frac{d[TA]_i}{dt} = \rho \left(J_{HA} + J_{A^-} \right),$$

$$\frac{d[H^+]_i}{dt} = \frac{2.303[H^+]_i}{\beta} \rho \left(\left(\frac{K_{HA}}{[H^+]_i + K_{HA} + K_{new}} \right) J_{HA} - \left(\frac{[H^+]_i}{[H^+]_i + K_{HA} + K_{new}} \right) J_{A^-} \right),$$

where

$$K_{\text{new}} = 2.303 K_{\text{HA}} \left(\frac{[\text{TA}]_\text{i}}{\beta} \right) \left(\frac{[\text{H}^+]_\text{i}}{[\text{H}^+]_\text{i} + K_{\text{HA}}} \right),$$

$$J_{\text{HA}} = P_{\text{HA}} \left([\text{HA}]_\text{o} - \frac{[\text{H}^+]_\text{i}}{[\text{H}^+]_\text{i} + K_{\text{HA}}} [\text{TA}]_\text{i} \right),$$

$$J_{\text{A}^-} = P_{\text{A}^-} \left(\frac{V_\text{m} F}{RT} \right) \left(\frac{[\text{A}^-]_\text{o} - \frac{K_{\text{HA}}}{[\text{H}^+]_\text{i} + K_{\text{HA}}} [\text{TA}]_\text{i} \epsilon}{1 - \epsilon} \right).$$

The first of these two equations is identical to that presented by BDW, whereas the second includes the new terms (K_{new}).

In the appendix of their paper, Keifer and Roos noted that it is possible to derive a comparable pair of equations for B/BH^+. In their 1981 review, Roos & Boron reported the two equations of the refined BDW model for B/BH^+ (see their Equation 25 and Equation 26):

$$\frac{\text{d}[\text{TB}]_\text{i}}{\text{d}t} = \rho \left(J_\text{B} + J_{\text{BH}^+} \right),$$

$$\frac{\text{d}[\text{H}^+]_\text{i}}{\text{d}t} = \frac{2.303 [\text{H}^+]_\text{i}}{\beta} \rho \left(\left(\frac{K_{\text{BH}^+}}{[\text{H}^+]_\text{i} + K_{\text{BH}^+} + K_{\text{new}}} \right) J_{\text{BH}^+} - \left(\frac{[\text{H}^+]_\text{i}}{[\text{H}^+]_\text{i} + K_{\text{BH}^+} + K_{\text{new}}} \right) J_\text{B} \right),$$

where

$$K_{\text{new}} = 2.303 K_{\text{HA}} \left(\frac{[\text{TA}]_\text{i}}{\beta} \right) \left(\frac{[\text{H}^+]_\text{i}}{[\text{H}^+]_\text{i} + K_{\text{HA}}} \right),$$

$$J_{\text{BH}^+} = P_{\text{BH}^+} \left(\frac{V_\text{m} F}{RT} \right) \left(\frac{[\text{BH}^+]_\text{o} - \frac{[\text{H}^+]_\text{i}}{[\text{H}^+]_\text{i} + K_{\text{BH}^+}} [\text{TB}]_\text{i} \epsilon'}{\epsilon' - 1} \right),$$

$$J_\text{B} = P_\text{B} \left([\text{B}]_\text{o} - \frac{K_{\text{BH}^+}}{[\text{H}^+]_\text{i} + K_{\text{BH}^+}} [\text{TB}]_\text{i} \right).$$

Note that as $[\text{TA}]_\text{i}$ approaches zero, or as β approaches infinity, the new terms (K_{new}) approach zero, and thus the refined BDW model collapses to the original BDW model. Keifer & Roos did not consider net H^+ efflux (*i.e.*, active acid extrusion).

In order to test whether the Keifer-Roos refinement really improves the predictions of the original BDW model, we implemented the BDW model with and without the Keifer-Roos refinement and employed the two models to simulate how pH_i changes when (a) only CO_2 enters the cell (*i.e.*, HCO_3^- permeability is zero) and (b) no proton pumping is present (*i.e.*, J_H is zero). With assumptions 'a' and 'b', the BDW model will take the system to equilibrium, where we can compare the predicted final pH_i with that produced by the Davenport diagram — our gold standard for the value of pH_i at equilibrium. Using the parameter values of Table 1 and Table 2, we find that both the refined BDW model and the Davenport diagram predict final pH_i values of 6.972, whereas the original BDW model predicts a slightly lower pH_i of 6.964 — lower because the original BDW does not incorporate as much self-buffering (as Keifer & Roos termed it).

Extending BDW to an epithelial cell. As part of their study of the CO_2 permeability of gastric-gland cells, Waisbren et al. (1994) extended the BDW model in three ways. First, rather than integrating two equations (*i.e.*, $\text{d}[\text{TA}]_\text{i}/\text{d}t$ and $\text{d}[\text{H}^+]_\text{i}/\text{d}t$), they integrated three equations (*i.e.*, $\text{d}[\text{HA}]_\text{i}/\text{d}t$, $\text{d}[\text{A}^-]_\text{i}/\text{d}t$, and $\text{d}[\text{H}+]_\text{i}/\text{d}t$). Second, after each step of the integration, they re-equilibrated HA, A^-, and H^+ in the cytosol — a maneuver equivalent to the Keifer-Roos extension of the BDW model. Third, they modelled two separate extracellular fluids (each an infinite reservoir), the equivalent of a luminal solution facing one half of the cell that represented the apical membrane, and a

basolateral solution facing the other half of the cell that represented the basolateral membrane. The geometry of the cell was still cylindrical, like the squid axon. In their review, Boron et al. (1994) provide additional information about this modelling, which showed that — to account for the physiological data in the paper by Waisbren et al. (1994) — the (membrane area) × (CO_2 permeability) product must be > 1000-fold greater for the basolateral than the apical side of the epithelial cell. Thus, this modelling was a critical part of the main conclusion of the paper by Waisbren et al. (1994), which identified the apical membranes of the gastric chief and parietal cells as the first known membranes with negligible CO_2 permeability.

Model of pH_i regulation by the Vaughan-Jones group. Following BDW's approach for modelling the net rate of acid addition into the cytosol, Leem et al. (1999) developed the first comprehensive mathematical model of pH_i regulation in cardiac myocytes. They simulated the experimentally observed pH_i recovery from an acid load (obtained with the ammonium prepulse technique, introduced by BDW) or a base load (obtained with the acetate-prepulse technique). In their model, Leem and coworkers incorporated acid-base fluxes mediated by four sarcolemma transporters, two acid extruders (*i.e.*, Na-H exchangers and Na/HCO_3 cotransporters) and two acid loaders (*i.e.*, Cl-HCO_3 exchangers and hypothetical Cl-OH exchangers) as well as a time-dependent intracellular buffering by the CO_2/HCO_3^- system. Their simulations nicely reproduced the pH_i changes that they observed in rather complex physiological experiments.

Model of H^+ diffusion by the Vaughan-Jones group. Richard Vaughan-Jones and his colleagues have extensively investigated the spatial variability of intracellular H^+ diffusion in a series of experimental studies (*e.g.*, confocal measurements of pH_i) complemented by mathematical modelling (Vaughan-Jones et al., 2002; Zaniboni et al., 2003; Swietach et al., 2003). These authors developed two-dimensional diffusion models of intracellular H^+ diffusion from a constant source to estimate the apparent diffusion constant of H^+ in cardiac ventricular myocytes. They found that the apparent H^+ mobility is low in cardiac cells because of the presence of mobile and immobile buffers. Later, Swietach and coworkers developed two-dimensional reaction-diffusion models, which they solved numerically in the longitudinal direction only (Swietach et al., 2003, 2005). This approach allowed them to investigate further the spatial variability of intracellular H^+ diffusion via a proposed H^+ shuttling among intracellular mobile buffers. More recently, this group developed a reaction-diffusion model of pH regulation in tumor spheroids to study the role of carbonic anhydrase (CA) IX in facilitating CO_2 excretion from tumor cells, thus favoring tumor-cell survival and proliferation (Swietach et al., 2008, 2009).

Models of the Gros group. Gerolf Gros and his colleagues have employed mathematical modelling of acid-base physiology to estimate the apparent membrane permeability of the red blood cell (RBC) membrane to CO_2 (P_{CO_2}) and HCO_3^- ($P_{HCO_3^-}$), as well as extra- and intracellular CA activity, from mass-spectrometric data and the ^{18}O-exchange technique (Wunder et al., 1997). Their compartmental model comprises a system of six ordinary differential equations that account for the ^{18}O-exchange reactions among HCO_3^-, CO_2 and H_2O in both the intracellular and extracellular compartments, and for transfer of CO_2 and H_2O across the intracellular and extracellular compartments.

In 2005, Endeward & Gros used this modelling framework to estimate P_{CO_2} and $P_{HCO_3^-}$ of the apical membrane of the colonic epithelium in guinea pigs. They found that the apical membrane has a quite low P_{CO_2}, possibly because of the absence of membrane proteins (*e.g.*, aquaporin 1, AQP1) that act as conduits (*i.e.*, gas channels) for the movement of CO_2.

In 2009, these same authors extended their previous compartmental model of ^{18}O-exchange to a one-dimensional reaction-diffusion model of an RBC surrounded by an extracellular unconvected layer that can exchange solutes with a well-stirred bulk solution (Endeward and Gros, 2009). They employed the model to assess the influence of intracellular and extracellular unconvected layers in the estimation of P_{CO_2} RBC membranes. The combination of physiological experiments and modelling allowed them to estimate the extra- and intracellular unstirred layers, and confirm their earlier conclusions that the P_{CO_2} of RBC membranes is low in the absence of gas channels.

Models of the CWRU group. With the goal of assessing the role of CO_2 channels in producing decreases in pH_i and transient alkaline transients in extracellular-surface pH (pH_S) as CO_2 enters a *Xenopus* oocyte (Endeward et al., 2006; Musa-Aziz et al., 2009a, 2010), the group at Case Western Reserve University developed a three-dimensional reaction-diffusion model of CO_2 influx into a spherical cell (Somersalo et al., 2012). The model accounts for a multitude of buffer reactions, as well as solute diffusion within the unconvected intracellular fluid (ICF) and the extracellular unconvected fluid (EUF) that surrounds the cell. Because the electrophysiologists established experimental conditions in which only CO_2 can cross the plasma membrane, the modellers allowed only CO_2 to diffuse between the ICF and EUF. However, all solutes can diffuse within the ICF as well as between the EUF and the bulk extracellular fluid (bECF) that surrounds the EUF. Somersalo and coworkers employed the model to investigate a variety of theoretical conditions. For example, they investigated how changes in the width of the EUF or in the value of P_{CO_2} affect pH_i and pH_S transients. The model suggests that, in oocytes, the background P_{CO_2} (*i.e.*, in the absence of channels) must be low in order for CO_2 channels to have the observed effect on the maximal rate of intracellular acidification, $(dpH_i/dt)_{max}$, or on the maximal height of the alkaline pH_S transient, $(\Delta pH_S)_{max}$.

In 2014, Occhipinti and coworkers extended the above theoretical model and employed it to investigate the role that CA II and CA IV play in enhancing transmembrane CO_2 fluxes (Musa-Aziz et al., 2014a,b; Occhipinti et al., 2014). The model was able to mimic the pH_i and pH_S experiments under a variety of experimental conditions. Moreover, it provided a novel observation that the effects on cytosolic CA II and extracellular CA IV on $(dpH_i/dt)_{max}$ and $(\Delta pH_S)_{max}$ are supra-additive. More recently, the CWRU group further extended the oocyte model to include the special microenvironment that the pH_S electrode creates when pushed against the oocyte membrane to record the pH_S transient (Calvetti et al., 2020). This model, solved using finite-element method, predicts that the special microenvironment between the blunt tip of the pH_S electrode and the oocyte membrane greatly amplifies the alkaline $(\Delta pH_S)_{max}$ as CO_2 enters the cell.

6 The Future

The advice, "It's tough to make predictions, especially about the future" is attributed to Yogi Berra, amateur philosopher and legend of American baseball. His advice certainly applies here. We imagine that the grand goal of the acid-base segment of world-wide biomedical science would be to model whole-body acid-base regulation on a cell-by-cell basis for a wide range of physiological and pathophysiological challenge. Of course, we all expect modelling to provide new insights that we can test in physiological experiments. However, the models should ultimately provide medical professionals with powerful insights into pathophysiology. These goals represent an enormous challenge in multi-scale modelling — multiscale in both time and space. That lofty goal is probably many decades away, even with appropriate grant support and continued development of computer hardware and software.

The process could begin at the single-cell level. Even here, the challenge is daunting because, as pointed out by Occhipinti and Boron (2015), the movements of acid-base equivalents across the plasma membrane create complex interdependencies among buffer reactions, diffusion processes and transporter mechanisms. Intuition alone cannot explain or predict the consequences of these numerous simultaneous processes on pH. Advanced mathematical models — including details on processes or more complex geometries — performed in conjunction with physiological experiments can provide a useful tool to make predictions and provide mechanistic explanations on observed pH changes. The pH community has begun taking the first steps with cells of simple geometry, like oocytes (*i.e.*, spheres). Even so, current models only simulate passive diffusion of substances like CO_2 and lactic acid. Current reaction-diffusion models do not yet incorporate electrodiffusion, let alone electrodiffusion through particular channels. The next step might be to incorporate specific acid-base transport systems (*e.g.*, Na/HCO_3 cotransporters, $Cl\text{-}HCO_3$ exchangers) with characteristic kinetic properties. Ultimately, one would like to include all traffic (*i.e.*, including non-acid-base traffic) across the cell membrane, and the regulation of this traffic. Model validation would require extensive physiological studies on these simple cell systems to verify

that simulations of ion conductances (and ultimately channels) and transporters are reasonable. Moreover, even these relatively simple first steps would require efficient computational methods for solving the governing equations.

From the level of the single cell, the field must move in two opposite directions. In the reductionist direction, we must move from whole cells to nanodomains (*i.e.*, the mesoscopic level) and ultimately to single molecules. At first, we guessed at even the number of different kinds of such proteins. Now we know the identities of specific proteins and their amino-acid sequences, and sometimes even their structures. Even so, cells are often capable of making many protein variants from one gene, and regulating these in response to myriad influences. Even the protein structures are merely an early step in understanding transporter mechanism.

In the opposite, integrative direction, the community must extend the models to more complex geometries, like the cells of a simple epithelium, spindle-shaped cells (*e.g.*, muscle), cylinders (*e.g.*, axons, dendritic processes), and ultimately cells of very complex geometry (*e.g.*, neurons, astrocytes). In real life, even a simple epithelium is far more complex than a cuboid. The apical membrane (nearest the tight junctions) of a cell of the proximal tubule (PT) has microvilli. The basolateral membrane (nearest the blood) has infoldings. These complexities create nanoenvironments on both the cytosolic and extracellular sides of the membrane. The tight junctions that separate the PT cells allow the paracellular diffusion of water and certain solutes. The lateral interspaces between adjacent cells also creates nanoenvironments. All of these nanoenvironments are likely to be extremely important for the physiology of the epithelium. Further complexities include the myriad cellular organelles. These not only affect diffusion of water and solutes through the cytosol (by creating tortuosity), but also can engage in their own collection of transport processes that can affect pH_i and contribute to buffering. Several groups have developed either steady-state or time-dependent compartmental models of acid-base transport in PTs and, more generally, solute reabsorption in various segments of the nephron (Thomas and Dagher, 1994; Krahn and Weinstein, 1996; Thomas et al., 2006; Weinstein et al., 2007; Weinstein and Sontag, 2009; Layton and Edwards, 2014; Edwards and Layton, 2017). Bransen and coworkers have used a finite-element approach to solve the partial differential equations that describe their reaction-diffusion model of Na-H exchange in the microvilli of the PT (Brasen et al., 2014).

Beyond cells, we must create whole tissues (*e.g.*, a cylindrical PT) from many cells, and create whole organs (*e.g.*, a kidney) from these tissues. Models of a whole kidney, for example, would have to consider the interstitial fluid and capillaries, the complex exchanges of substances among them, and the changes in composition that occur as fluids flow along the lumens of the tubule and capillaries. Comparable modelling must extend to every tissue and organ, and consider the complex intercommunications among them via the circulatory and neuro-endocrine systems as well as metabolism. In the case of acid-base physiology, one must model the specific roles that certain organs — the brain, the pulmonary system, and the kidneys — play in whole-body pH regulation.

All along the way, community members must cooperate because no one group of investigators can possibly accomplish the ultimate goal single-handedly. The models must be open source, modular and sharable — and the community must share. Finally, in order for modelling approaches to be consistent, the community must establish standard approaches for gathering physiological data, and agree on standard values for physiological parameters. Here, an organisation like the International Union of Physiological Sciences (IUPS)[22] can play a critical role.

7 Acknowledgements

Supported by National Institute of Health (NIH) grants K01-DK107787 (to RO), U01GM111251 and DK113197 (to WFB), Office of Naval Research (ONR) grant N00014-15-1-2060 (to WFB), and a Multidisciplinary University Research Initiative (MURI) grant N00014-16-1-2535 from the DoD (to WFB). WFB gratefully acknowledges the support of the Myers/Scarpa endowed chair. SS acknowledges the financial support provided by the Aotearoa Foundation.

[22] http://www.iups.org/

8 Conflict of Interests

None declared.

References

F. T. Bergmann, D. Nickerson, D. Waltemath, and M. Scharm. SED-ML web tools: generate, modify and export standard-compliant simulation studies. *Bioinformatics (Oxford, England)*, 33 (8):1253–1254, 2017. ISSN 1367-4811.

M. O. Bevensee and W. F. Boron. Manipulation and regulation of cytosolic pH. In *Measurement and Manipulation of Intracellular Ions, Jacob Kracicer & Jeffrey Dixon, Eds.*, volume 27 of *Methods in Neurosciences*, pages 252–273. Academic Press, San Diego CA, 1995.

M. O. Bevensee and W. F. Boron. Control of intracellular pH. In *Seldin and Giebisch's The Kidney: Physiology & Pathophysiology*, volume 2, pages 1773–1835. Academic Press, 5th edition, 2013.

W. F. Boron. Intracellular pH transients in giant barnacle muscle fibers. *American Journal of Physiology*, 233(3):C61–73, 1977. ISSN 0002-9513.

W. F. Boron. Regulation of intracellular pH. *Advances in Physiology Education*, 28(1):160–179, 2004. ISSN 1043-4046.

W. F. Boron. Sharpey-Schafer lecture: gas channels. *Experimental Physiology*, 95(12):1107–1130, 2010. ISSN 1469-445X.

W. F. Boron and E. L. Boulpaep, editors. *Medical Physiology*. Elsevier, Philadelphia, PA, 3rd edition edition, 2016. ISBN 978-1-4557-4377-3.

W. F. Boron and P. De Weer. Intracellular pH transients in squid giant axons caused by CO, NH, and metabolic inhibitors. *Journal of General Physiology*, 67(1):91–112, 1976. ISSN 0022-1295.

W. F. Boron and A. Roos. Comparison of microelectrode, DMO, and methylamine methods for measuring intracellular pH. *American Journal of Physiology*, 231(3):799–809, 1976. ISSN 0002-9513.

W. F. Boron, W. C. McCormick, and A. Roos. pH regulation in barnacle muscle fibers: dependence on intracellular and extracellular pH. *American Journal of Physiology*, 237(3):C185–193, 1979. ISSN 0002-9513.

W. F. Boron, S. J. Waisbren, I. M. Modlin, and J. P. Geibel. Unique permeability barrier of the apical surface of parietal and chief cells in isolated perfused gastric glands. *The Journal of Experimental Biology*, 196:347–360, 1994. ISSN 0022-0949.

J. C. Brasen, J. L. Burford, A. A. McDonough, N.-H. Holstein-Rathlou, and J. Peti-Peterdi. Local pH domains regulate NHE3-mediated Na reabsorption in the renal proximal tubule. *American Journal of Physiology - Renal Physiology*, 307(11):F1249–1262, 2014. ISSN 1522-1466.

J. N. Brönsted. Einige Bemerkungen über den Begriff der Säuren und Basen. *Recueil des Travaux Chimiques des Pays-Bas*, 42(8):718–728, 1923. ISSN 0165-0513.

D. Calvetti, J. Prezioso, R. Occhipinti, W. F. Boron, and E. Somersalo. Computational model of electrode-induced microenvironmental effects on pH measurements near a cell membrane. *SIAM Multiscale Modeling & Simulation*, (in press), 2020.

A. A. Cuellar, C. M. Lloyd, P. F. Nielsen, D. P. Bullivant, D. P. Nickerson, and P. J. Hunter. An overview of CellML 1.1, a biological model description language. *Simulation*, 79(12):740–747, 2003. ISSN 0037-5497.

A. Edwards and A. T. Layton. Cell volume regulation in the proximal tubule of rat kidney. *Bulletin of Mathematical Biology*, 79(11):2512–2533, 2017. ISSN 1522-9602.

V. Endeward and G. Gros. Extra- and intracellular unstirred layer effects in measurements of CO_2 ^{18}O technique for red blood cells. *The Journal of Physiology*, 587(Pt 6):1153–1167, 2009. ISSN 1469-7793.

V. Endeward, R. Musa-Aziz, G. J. Cooper, L. M. Chen, M. F. Pelletier, L. V. Virkki, C. T. Supuran, L. S. King, W. F. Boron, and G. Gros. Evidence that aquaporin 1 is a major pathway for CO transport across the human erythrocyte membrane. *The FASEB Journal*, 20(12):1974–1981, 2006. ISSN 1530-6860.

D. E. Goldman. Potential, impedance, and rectification in membranes. *Journal of General Physiology*, 27(1):37–60, 1943.

H. S. Harned and R. Davis. The ionization constant of carbonic acid in water and the solubility of carbon dioxide in water and aqueous salt solutions from 0 to 50°. *Journal of the American Chemical Society*, 65(10):2030–2037, 1943. ISSN 0002-7863.

L. J. Henderson. Blood as a Physicochemical System. *Journal of Biological Chemistry*, 46(2): 411–419, 1921. ISSN 0021-9258, 1083-351X.

A. L. Hodgkin and A. F. Huxley. A quantitative description of membrane current and its application to conduction and excitation in nerve. *The Journal of Physiology*, 117(4):500–544, 1952.

M. H. Jacobs. Some aspects of cell permeability to weak electrolytes. In *Cold Spring Harbor Symposia on Quantitative Biology*, volume 8, pages 30–39. Cold Spring Harbor Laboratory Press, 1940.

D. W. Keifer and A. Roos. Membrane permeability to the molecular and ionic forms of DMO in barnacle muscle. *American Journal of Physiology*, 240(1):C73–79, 1981. ISSN 0002-9513.

K. Koppel, M. & Spiro. Über die Wirkung von Moderatoren (Puffern) bei der Verschiebung des Säure-Basengleichgewichtes in biologischen Flüssigkeiten. *Biochemische Zeitung*, 65:409–439, 1914.

T. A. Krahn and A. M. Weinstein. Acid/base transport in a model of the proximal tubule brush border: impact of carbonic anhydrase. *American Journal of Physiology - Renal Physiology*, 270(2): F344–F355, 1996. ISSN 1931-857X, 1522-1466.

A. T. Layton and A. Edwards. *Mathematical Modeling in Renal Physiology*. Lecture Notes on Mathematical Modelling in the Life Sciences. Springer-Verlag, Berlin Heidelberg, 2014.

C. H. Leem, D. Lagadic-Gossmann, and R. D. Vaughan-Jones. Characterization of intracellular pH regulation in the guinea-pig ventricular myocyte. *The Journal of Physiology*, 517 (Pt 1):159–180, 1999. ISSN 0022-3751.

M. D. Milne, B. H. Scribner, and M. A. Crawford. Non-ionic diffusion and the excretion of weak acids and bases. *The American Journal of Medicine*, 24(5):709–729, 1958. ISSN 0002-9343.

R. Musa-Aziz, L. M. Chen, M. F. Pelletier, and W. F. Boron. Relative CO/NH selectivities of AQP1, AQP4, AQP5, AmtB, and RhAG. *Proceedings of the National Academy of Sciences of the United States of America*, 106(13):5406–5411, 2009a. ISSN 1091-6490.

R. Musa-Aziz, L. Jiang, L. M. Chen, K. L. Behar, and W. F. Boron. Concentration-dependent effects on intracellular and surface pH of exposing *Xenopus* oocytes to solutions containing NH_3/NH_4^+. *The Journal of Membrane Biology*, 228(1):15–31, 2009b. ISSN 1432-1424.

R. Musa-Aziz, W. F. Boron, and M. D. Parker. Using fluorometry and ion-sensitive microelectrodes to study the functional expression of heterologously-expressed ion channels and transporters in *Xenopus* oocytes. *Methods*, 51(1):134–145, 2010. ISSN 1095-9130.

R. Musa-Aziz, R. Occhipinti, and W. F. Boron. Evidence from simultaneous intracellular- and surface-pH transients that Carbonic Anhydrase II enhances CO_2 fluxes across *Xenopus* oocytes plasma membranes. *American Journal of Physiology - Cell Physiology*, 307(9):C791–813, 2014a. ISSN 1522-1563.

R. Musa-Aziz, R. Occhipinti, and W. F. Boron. Evidence from simultaneous intracellular- and surface-pH transients that Carbonic Anhydrase IV enhances CO_2 fluxes across *Xenopus* oocyte plasma membranes. *American Journal of Physiology - Cell Physiology*, 307(9):C814–840, 2014b. ISSN 1522-1563.

R. Occhipinti and W. F. Boron. Mathematical modeling of acid-base physiology. *Progress in Biophysics and Molecular Biology*, 117(1):43–58, 2015. ISSN 1873-1732.

R. Occhipinti, R. Musa-Aziz, and W. F. Boron. Evidence from mathematical modeling that Carbonic Anhydrase II and IV enhance CO fluxes across *Xenopus* oocytes plasma membranes. *American Journal of Physiology - Cell Physiology*, 307(9):C841–858, 2014. ISSN 1522-1563.

J. Orloff and R. W. Berliner. The mechanism of the excretion of ammonia in the dog. *The Journal of Clinical Investigation*, 35(2):223–235, 1956. ISSN 0021-9738.

A. Roos. Intracellular pH and intracellular buffering power of the cat brain. *American Journal of Physiology*, 209(6):1233–1246, 1965. ISSN 0002-9513.

A. Roos. Intracellular pH and distribution of weak acids across cell membranes. A study of D- and L-lactate and of DMO in rat diaphragm. *The Journal of Physiology*, 249(1):1–25, 1975. ISSN 0022-3751.

A. Roos and W. F. Boron. The buffer value of weak acids and bases: origin of the concept, and first mathematical derivation and application to physico-chemical systems. The work of M. Koppel and K. Spiro (1914). *Respiration Physiology*, 40(1):1–32, 1980. ISSN 0034-5687.

A. Roos and W. F. Boron. Intracellular pH. *Physiological Reviews*, 61(2):296–434, 1981. ISSN 0031-9333.

E. Somersalo, R. Occhipinti, W. F. Boron, and D. Calvetti. A reaction-diffusion model of CO_2 influx into an oocyte. *Journal of Theoretical Biology*, 309:185–203, 2012. ISSN 1095-8541.

P. Swietach, M. Zaniboni, A. K. Stewart, A. Rossini, K. W. Spitzer, and R. D. Vaughan-Jones. Modelling intracellular H^+ ion diffusion. *Progress in Biophysics and Molecular Biology*, 83(2): 69–100, 2003. ISSN 0079-6107.

P. Swietach, C.-H. Leem, K. W. Spitzer, and R. D. Vaughan-Jones. Experimental generation and computational modeling of intracellular pH gradients in cardiac myocytes. *Biophysical Journal*, 88(4):3018–3037, 2005. ISSN 0006-3495.

P. Swietach, S. Wigfield, P. Cobden, C. T. Supuran, A. L. Harris, and R. D. Vaughan-Jones. Tumor-associated carbonic anhydrase 9 spatially coordinates intracellular pH in three-dimensional multicellular growths. *The Journal of Biological Chemistry*, 283(29):20473–20483, 2008. ISSN 0021-9258.

P. Swietach, S. Patiar, C. T. Supuran, A. L. Harris, and R. D. Vaughan-Jones. The role of carbonic anhydrase 9 in regulating extracellular and intracellular pH in three-dimensional tumor cell growths. *The Journal of Biological Chemistry*, 284(30):20299–20310, 2009. ISSN 0021-9258.

S. P. L. Sørensen. *Über die Messung und die Bedeutung der Wasserstoffionenkonzentration bei enzymatischen Prozessen*. Universitätsbibliothek Johann Christian Senckenberg, 1909.

S. R. Thomas and G. Dagher. A kinetic model of rat proximal tubule transport—Load-dependent bicarbonate reabsorption along the tubule. *Bulletin of Mathematical Biology*, 56(3):431–458, 1994. ISSN 0092-8240.

S. R. Thomas, A. T. Layton, H. E. Layton, and L. C. Moore. Kidney modeling: Status and perspectives. *Proceedings of the IEEE*, 94(4):740–752, 2006. ISSN 0018-9219.

D. D. Van Slyke. On the measurement of buffer values and on the relationship of buffer value to the dissociation constant of the buffer and the concentration and reaction of the buffer solution. *Journal of Biological Chemistry*, 52(2):525–570, 1922. ISSN 0021-9258, 1083-351X.

R. D. Vaughan-Jones, B. E. Peercy, J. P. Keener, and K. W. Spitzer. Intrinsic H^+ ion mobility in the rabbit ventricular myocyte. *The Journal of Physiology*, 541(Pt 1):139–158, 2002. ISSN 0022-3751.

S. J. Waisbren, J. P. Geibel, I. M. Modlin, and W. F. Boron. Unusual permeability properties of gastric gland cells. *Nature*, 368(6469):332–335, 1994. ISSN 0028-0836.

A. M. Weinstein and E. D. Sontag. Modeling proximal tubule cell homeostasis: Tracking changes in luminal flow. *Bulletin of Mathematical Biology*, 71(6):1285–1322, 2009. ISSN 1522-9602.

A. M. Weinstein, S. Weinbaum, Y. Duan, Z. Du, Q. Yan, and T. Wang. Flow-dependent transport in a mathematical model of rat proximal tubule. *American Journal of Physiology - Renal Physiology*, 292(4):F1164–1181, 2007. ISSN 1931-857X.

M. Wunder, P. Böllert, and G. Gros. Mathematical modelling of the role of intra- and extracellular activity of carbonic anhydrase and membrane permeabilities of HCO, HO and CO in ^{18}O exchange. *Isotopes in Environmental and Health Studies*, 33(1):197–205, 1997. ISSN 1025-6016.

M. Zaniboni, P. Swietach, A. Rossini, T. Yamamoto, K. W. Spitzer, and R. D. Vaughan-Jones. Intracellular proton mobility and buffering power in cardiac ventricular myocytes from rat, rabbit, and guinea pig. *American Journal of Physiology-Heart and Circulatory Physiology*, 285(3): H1236–H1246, 2003. ISSN 0363-6135.

Reproducibility report for: The Boron & De Weer Model of Intracellular pH Regulation
Submitted to: *Physiome*
Manuscript number/identifier: S000002

Curation outcome summary: Successfully reproduced Figure 4 and 6 as presented in this manuscript.

Box 1: Criteria for repeatability and reproducibility

- ■ **Model source code provided:**
  - ☐ Source code: a standard procedural language is used (e.g. MATLAB, Python, C)
    - ☐ There are details/documentation on how the source code was compiled
    - ☐ There are details on how to run the code in the provided documentation
    - ☐ The initial conditions are provided for each of the simulations
    - ☐ Details for creating reported graphical results from the simulation results
  - ■ Source code: a declarative language is used (e.g. SBML, CellML, NeuroML)
    - ■ The algorithms used are defined or cited in previous articles
    - ■ The algorithm parameters are defined
    - ■ Post-processing of the results are described in sufficient detail
- ☐ **Executable model provided:**
  - ☐ The model is executable without source (e.g. desktop application, compiled code, online service)
    - ☐ There are sufficient details to repeat the required simulation experiments
- ■ **The model is described mathematically in the article(s):**
  - ■ Equations representing the biological system
  - ■ There are tables or lists of parameter values
  - ■ There are tables or lists of initial conditions
  - ☐ Machine-readable tables of parameter values
  - ☐ Machine-readable tables of initial conditions
- ■ **The simulation experiments using the model are described mathematically in the article:**
  - ■ Integration algorithms used are defined
  - ☐ Stochastic algorithms used are defined
  - ☐ Random number generator algorithms used are defined
  - ☐ Parameter fitting algorithms are defined
  - ☐ The paper indicates how the algorithms yield the desired output

Box 2: Criteria for accessibility

- ■ Model/source code is available at a public repository or researcher's web site
  - ☐ Prohibitive license provided
  - ☐ Permissive license provided
  - ■ Open-source license provided
- ■ All initial conditions and parameters are provided
- ■ All simulation experiments are fully defined (events listed, collection times and measurements specified, algorithms provided, simulator specified, etc.)

Box 3: Rules for Credible practice of Modeling and Simulation[a]

[a]Model credibility is assessed using the Interagency Modeling and Ananlysis Group conformance rubric: https://www.imagwiki.nibib.nih.gov/content/10-simple-rules-conformance-rubric

- ■ Define context clearly: Extensive
- ■ Use appropriate data: Extensive
- ■ Evaluate within context: Extensive
- ☐ List limitations explicitly: Insufficient
- ■ Use version control: Extensive
- ■ Document adequately: Extensive
- ■ Conform to standards: Extensive

Box 4: Evaluation

- ■ Model and its simulations could be repeated using provided declarative or procedural code
- ■ Model and its simulations could be reproduced

Summary comments: Model and source code are available in the associated OMEX archive. This was used in our attempt to reproduce the results presented in the paper. We successfully ran the SED-ML model files to reproduce Figure 4 and 6 as presented in this manuscript.

Anand K. Rampadarath[1], PhD
Curator
Center for Reproducible Biomedical Modeling

David P. Nickerson, PhD
Curation Service Director
Center for Reproducible Biomedical Modeling

Auckland Bioengineering Institute,
University of Auckland

[1]Email: a.rampadarath@auckland.ac.nz